Results in Engineering 26 (2025) 104739

Contents lists available at ScienceDirect

Results in Engineering

journal homepage: www.sciencedirect.com/journal/results-in-engineering

Research paper

Electro-osmotic peristaltic streaming of a fractional second-grade viscoelastic nanofluid with single and multi-walled carbon nanotubes in a ciliated tube

Mahadev M Channakote [a,*], Shekar Marudappa [b], O. Anwar Bég [c], Mahesha Narayana [d], C. Siddabasappa [e]

[a] Department of Mathematics and Statistics, M. S. Ramaiah University of Applied Science, Bengaluru, Karnataka, 560054, India
[b] Department of Mathematics, B. M. S. College of Engineering, Bengaluru, Karnataka, 560019, India
[c] Multi-Physical Engineering Sciences Group, Mechanical Engineering Department, Corrosion/Coating Lab., 3-08, SEE Building, University of Salford, Manchester, M54WT, UK
[d] Department of Mathematics, The University of the West Indies, Mona Campus, Kingston, Jamaica
[e] Department of Sciences and Humanities, CHRIST University, Bengaluru, Karnataka, 560074, India

ARTICLE INFO

Keywords:
Thermal conductivity
Carbon nanotubes
Electro-osmosis
Debye–Huckel linearization
Thermal buoyancy
Cilia

ABSTRACT

Mathematical modeling of carbon nanotubes (CNTs) in biological fluids is essential for drug delivery, biosensing, and targeted therapy. This study explores the transport dynamics of single-walled carbon nanotubes (SWCNTs) and multi-walled carbon nanotubes (MWCNTs) based nanofluids under electro-osmotic peristaltic flow influenced by ciliary motion. A microfluidic channel lined with cilia, hair-like structures found in human airways and reproductive tracts, is considered. The coordinated beating of cilia generates a wavelike motion that propels the surrounding biological fluid. When an electric field is applied across the channel, electro-osmotic forces further modify the flow, affecting velocity and temperature distribution. A nanofluid, consisting of CNTs suspended in a base fluid, flows through this cilia-driven microchannel. The transport process is governed by electro-osmosis, heat transfer, and thermal radiation effects, with simplifications based on long-wavelength and low Reynolds number assumptions. The Caputo fractional model and Debye–Hückel linearization are used to analyze the interaction between electro-osmotic forces and thermal-mechanical effects. The results reveal that the negative Helmholtz-Smoluchowski parameter (U_{hs}) reduces the axial velocity in the core whereas it increases in the periphery of the channel, while the opposite trend is observed for positive U_{hs}. Longer cilia (β) and higher electro-osmotic parameter (m) slow the core flow while accelerating peripheral transport. Thermal effects indicate that an increased heat source (B) raises temperature and axial velocity, whereas a higher nanotube volume fraction (ϕ) enhances axial velocity but reduces temperature. Notably, *MWCNTs* exhibit superior axial velocity and temperature enhancement compared to SWCNTs. *These outcomes provide valuable insights into electro-osmotic cilia-driven nanofluid transport, offering a theoretical foundation for optimizing microfluidic and biomedical applications.*

1. Introduction

Peristaltic flow, driven by rhythmic tube contractions, is vital in biological fluid transport, like in the gut and capillaries. This mechanism has engineering, biomedical, and industrial applications. Researchers study peristalsis to improve artificial fluid transport, leading to innovations. Peristaltic micro-pumps and bio-inspired systems aid drug delivery and blood circulation in medical devices. Lab-on-a-chip tech uses it for precise diagnostics. Compact peristaltic channels help cool electronics. In industries with strict hygiene rules, peristaltic systems ensure sterile fluid handling. These systems are also tested in renewable energy technologies. Although peristaltic mechanisms were recognized in physiology long ago, mathematical studies on the subject began in the 1960s with the application of the Navier-Stokes equations for viscous fluids. Notable contributions were made by Yin and Fung [1], as well as Shapiro et al. [2]. They introduced lubrication approximations and transformed the moving frame of reference into a stationary (wave) frame of reference, significantly simplifying the mathematics involved in peristaltic transport. Since then, many researchers have adopted this

* Corresponding author.
E-mail address: mchannakote@rediffmail.com (M.M. Channakote).

https://doi.org/10.1016/j.rineng.2025.104739
Received 9 February 2025; Received in revised form 16 March 2025; Accepted 26 March 2025
Available online 30 March 2025

Nomenclature

$\widetilde{U}$ and $\widetilde{W}$	velocity components in fixed frame
u and w	velocity component in wave frame
μ_{nf}	viscosity of the nano liquid
ρ_{nf}	effective density
k_{nf}	thermal conductivity
$(cp)_{nf}$	specific heat
α_{nf}	thermal expansion coefficient
ϕ	volume fraction of nanoparticle
ρ_e	the charge density
ε_r	relative permittivity of the medium
ε_0	permittivity of the vacuum
n^+, n^-	cation and anion densities
Φ	electric potential
E_R and E_z	the electric body force in the radial and axial co-ordinates
Br	Brinkman number
U_{hS}	electro-osmotic parameter
m	Debye–Huckle parameter
Q	the time-averaged flow rate
β	cilia length
B	thermal source/sink parameter
Gr	Grashof number

approach, particularly in situations where the fluid being pumped must remain uncontaminated, such as blood, or non-corrosive, ensuring that it does not interact with the components of conventional pumping devices. Ary (wave) frame of reference to greatly simplify the mathematics of peristaltic transport. Subsequently, numerous researchers have adopted this concept and applied it in scenarios where the pumped fluid needs to remain uncontaminated, such as in the case of blood, or be non-corrosive, ensuring it does not come into contact with the working components of typical pumping devices. A noteworthy number of researchers have been investigating peristaltic transport phenomena across diverse geometries in recent years, owing to their practical applications in manufacturing and magnetic industries. Rathod and Channakote [3] explored the impact of permeability on peristaltic transport in viscous fluids, modeling ureteral dynamics. Narla et al. [4] applied the Jeffrey's elastic-viscous model to simulate unsteady magnetized pumping in a curved conduit influenced by peristaltic waves. Their study focused on the effects of curvature parameters, the ratio of relaxation to retardation time (the first viscoelastic parameter of Jeffrey), and the Hartmann number (which represents the magnetic field) on radial velocity distributions, bolus dynamics, and the characteristics of trapping and reflux. Ajithkumar et al. [5] investigated the application of biomimetic pumps for handling dangerous substances, examining the catalytic effects on the peristaltic movement of Jeffrey fluid through a flexible porous channel under an inclined magnetic field. Rathod and Mahadev [6] conducted a study on how ureteral peristalsis -wave-like contractions of the ureter that propel urine from the kidneys to the bladder is affected by a magnetic field. Their investigation explored the interaction between the physiological mechanism of peristalsis and external magnetic forces, aiming to understand whether and how magnetic fields might influence fluid movement or the behavior of smooth muscles within the ureter. An additional study by Hayat [7] explored how silver nanoparticles contribute to thermal energy processes that are influenced by peristalsis. The study by Choudhari et al. [8] focused on the peristaltic blood flow mechanism, investigating it through the lens of non-Newtonian fluids and the variability of liquid characteristics; Tripathi et al. [9], who employed differential transform methods to analyze asymmetric peristaltic propulsion in tubes filled with fractional Oldroyd-B viscoelastic-saturated Darcy-Brinkman porous media; and Ali et al. [10], who utilized a forward time center space finite difference method to examine carreau fluid pumping in curved ducts.

Furthermore bio-heat transfer in blood flow and peristaltic transport has widespread applications in medical treatments, drug delivery, diagnostics, and artificial organ development. Advanced modeling techniques enhance the precision of biomedical devices and therapies, improving patient outcomes in various healthcare fields. Bio-heat transport principles aid in designing efficient dialysis machines and extracorporeal blood circulation systems, preventing thermal imbalances. Dolat Khan et al. [11,12] investigated the generalized two-phase free convection flow of a dusty Jeffrey fluid between two infinite vertical parallel plates, with a primary focus on heat transfer. They employed Caputo-Fabrizio time-fractional derivatives to describe the behavior of the dusty Jeffrey fluid. In a separate study, researchers analyzed the effectiveness of heat transfer and the corresponding entropy generation in a generalized dusty tetra-hybrid nanofluid within a microchannel. The flow in this scenario is governed by free convection and buoyant forces, which play a crucial role in the heat transfer process. Peristaltic motion in the intestines influences heat exchange, impacting digestion, metabolic reactions, and drug absorption. Peristaltic flow models play a vital role in exploring heat transport, particularly in therapies like cancer hyperthermia, where controlled heat is applied to tissues. Additionally, heat-enhanced drug diffusion in peristaltic flow supports the targeted delivery of temperature-sensitive therapeutic agents. Asha and Deepa [13] studied entropy generation in peristaltic blood flow of a magneto-micropolar fluid in a tapered asymmetric channel with thermal radiation. Their research is important for understanding energy dissipation and fluid transport in biomedical and industrial applications, optimizing hemodynamic conditions, and improving efficiency in magnetohydrodynamic (MHD) fluid systems. Mahadev and Kalse [14] analyzed convective heat transfer and viscous dissipation in peristaltic flow of Ellis fluid through a non-uniform tube, highlighting its relevance in non-Newtonian fluid dynamics for biological and industrial applications. The study by Imran et al. [15] focused on the examination of radiative heat transfer in the flow of electro-osmotic magneto-Nano fluids driven by ciliary propulsion. Some latest research articles related the heat transfer system for various fluids flow systems are provided in [16–20].

Nanoparticle research in fluid mechanics has surged in the 21st century due to applications in medicine, energy, propulsion, lubricants, and bioengineering. Their nanoscale properties significantly impact fluid dynamics, offering advantages over traditional fluids. Mathematical modeming and experiments are key to understanding and optimizing their potential in various fields. Nano fluids, colloidal suspensions of nanoparticles in base fluids, have emerged as a promising medium for enhancing heat transfer and fluid transport due to their superior thermal and rheological properties, making them promising candidates in many emerging technologies including cancer treatment, sterilization of biological devices, renewable energy, space propulsion (rocket fuel gels), industrial coolants and lubricants. The integration of nanofluids with engineered peristaltic systems holds significant potential for advancements in various industrial sectors, including medical devices, soft robotics, materials processing, manufacturing, and environmental protection. This is due to the ability to utilize the unique properties of nanoparticles to enhance fluid dynamics and heat transfer processes. Nowadays, the study of Nano fluid has gained great interest due to its medical, industrial, and biological applications. Some studies relating to the peristaltic flow of Newtonian and non-Newtonian fluids are given in Refs [21–24]. Choi [25] introduced the term "nanofluid" to describe a mixture of a base fluid and nanoparticles that possess distinctive chemical and physical characteristics. Buongiorno [26] suggested that thermophoresis and Brownian motion play crucial roles in the dynamics of Nano fluids. He developed a two-component nanoscale model that takes into account both thermal diffusion and mass diffusion (nanoparticle concentration). In essence, a nanofluid is a liquid suspension made up of tiny particles that are <100 nanometres in diameter. These particles are typically composed of non-metals like graphite and carbon nanotubes, or metals such as carbides, nitrides, and oxides. Several researchers have therefore investigated theoretically and computationally peristaltic flows of nanofluids motivated by biomedical and energy device applications. The study of peristaltic flow has advanced with nanotechnology, particularly through Nano fluids-suspensions of nanoparticles in base fluids. These fluids enhance thermal conductivity, viscosity, and heat transfer. Integrating peristaltic flow with Nano fluids has expanded possibilities for efficient transport in micro- and nano-scale systems. Tripathi and Bég [27] conducted one of the earliest studies on the peristaltic propulsion of nanofluids, focusing on applications in pharmacodynamics. They utilized Buongiorno's model to analyze how various factors, such as thermal and species Grashof numbers, Brownian motion, and thermophoretic body force parameters, influence the distributions of velocity, nanoparticle fraction, temperature, and pressure gradients. Nadeem et al. [28] applied the homotropy perturbation method (HPM) to investigate the peristaltic flow of a nanofluid through eccentric tubes containing Darcian porous media. Their findings indicated that pressure rise is reduced with an increase in the thermal Grashof number, while it is enhanced with a higher peristaltic wave amplitude ratio in the retrograde pumping zone. Conversely, the opposite effect was observed in the peristaltic pumping and augmented pumping zones. Additional research on the mechanics of peristaltic nanofluids includes work by Tripathi et al. [29], who explored the effects of unsteady and finite length conditions in nanofluid peristaltic micro-pumps, and Prakash et al. [30], who examined the impacts of thermal radiation and viscosity variations in magnetic nanoparticle-infused solar collector fluids. Collectively, these studies confirmed a significant enhancement in thermal properties and demonstrated that optimized hydromechanical peristaltic pumping efficiency can be achieved through careful selection of nanoparticle volume fractions.

Various nanostructures, including carbon nanotubes (CNTs) like single-walled (SWCNTs) and multi-walled (MWCNTs), have been synthesized and studied for their exceptional thermal conductivity and mechanical strength. Incorporating CNTs into viscoelastic fluids can improve their performance for advanced engineering and biomedical applications [31–33]. These nanostructures, such as nano-shells, nano-dots, and nanowires, have diverse industrial applications, from aerospace to biomedical systems. CNTs, with their superior thermal properties and structural stability, can enhance the thermal characteristics of materials like fluids and solids. Their unique properties make them ideal for improving thermo-fluid performance in various applications, including coating systems and tissue engineering. CNT-based nanofluids have been investigated for peristaltic systems, showing promising results in enhancing fluid flow and viscosity. Studies have demonstrated the potential of CNTs, particularly SWCNTs, in improving the efficiency of peristaltic transport and fluid dynamics in biomedical applications. Nadeem and Sadaf [34] conducted a study on the peristaltic transport of a hybrid nanofluid with varying viscosity in a curved duct, using single-walled carbon nanotubes (SWCNT) and multi-walled carbon nanotubes (MWCNT) in water. Iqra Shahzadi et al. [35] investigated the peristaltic flow of nanofluid through a permeable-walled annulus, analyzing the effect of single-walled carbon nanotubes (SWCNT) on effective viscosity. They observed a significant increase in SWCNT-blood flow with higher viscosity parameters, as well as an improvement in the pressure differential within the annulus.

Cilia are tiny hair-like structures found in various biological systems, such as the respiratory tract, reproductive organs, and gastrointestinal lining, respiratory tract, kidneys, nasal passages, and lungs, among other organs, where they support vital processes. Their coordinated beating creates intricate wave patterns that are essential for peristaltic transport, which moves fluids, mucus, or particles through narrow channels. This mechanism is vital for functions like clearing mucus in the lungs, moving cerebrospinal fluid in the brain, and transporting eggs in the fallopian tubes. In addition to peristalsis, nature exhibits various other propulsion mechanisms. Ciliary motion can be categorized into two main wave patterns: Metachronal Waves, where successive cilia beat in a coordinated wave-like sequence to propel fluids efficiently with minimal energy loss, and symplectic and antipleptic waves, involving synchronized or opposite-phase motion of neighboring cilia to regulate flow rate and mixing efficiency. Complex cilia waves improve the efficiency, control, and adaptability of biological peristaltic mechanisms. The integration of cilia dynamics with electro-osmotic effects, heat transfer, and nanotechnology presents new opportunities in biomedical engineering, drug delivery, and artificial organ development. Understanding these dynamics is crucial for advancing bio-inspired fluid transport systems in medical and industrial applications. One particularly efficient method is known as cilia-driven flow [36]. All mammalian cells feature these tiny, hair-like structures on their surfaces, which are essential for many physiological functions in the human body. Mathematical modeling interest in cilia-driven flows emerged in the 1970s with the pioneering studies of Blake [37] who developed an elliptical cilia-beating model, valid for metachronal propulsion in which the cilia drive fluid in a particular direction and there is an effective stroke followed by a recovery stroke. The flow is therefore generated due to a metachronal wave propagation which is produced by the collective, rhythmic beating of the cilia with constant wave speed. This initial work was however confined to Newtonian viscous fluids. Much later interest emerged in generalizing Blake's approach to non-Newtonian liquids, which have diverse applications in for example cilia-assisted micro-duct propulsion, bio-micro-mechanical systems etc. Almheidat et al. [38] conducted a study on thermal analysis using Prandtl nanofluid in a non-uniform channel. The study focused on complex cilia waves in a computational paradigm.

Ramesh et al. [39] studied the magneto-hydrodynamic propulsion of cilia in Stokesian couple stress fluids in a conduit. They found that increasing cilia length led to a slight increase in maximum shear stress at the inner walls but a significant decrease in troughs. Additionally, they observed that cilia length had a greater impact on volumetric flow rates compared to cilia eccentricity. A recent analysis and references on this topic can be found in [40–49].

Electro-osmosis is the process by which an ionic liquid moves through a capillary or other porous material under the action of an applied electric field, which may be static or alternating in nature. Electro-osmotic flow may be impacted by the fluidic ion content. In recent years a number of researchers have combined electro-osmotic flows with peristaltic pumping mechanisms, owing to emerging applications in bio-microfluidics. The overall transport qualities of the peristaltic system can be influenced by the way ions travel in response to an electric field. Electro-osmosis can be used to boost the flow rate in peristaltic systems. An electric field applied perpendicular to the flow direction can induce electro-osmotic flow in addition to peristaltic flow, resulting in increased fluid velocity. Better control over the fluid behavior is made possible by the interaction of the electro-osmotic and peristaltic effects. The direction and speed of fluid flow may be adjusted using the electric field, giving further control over the transport process. Early work in electro-osmotic peristalsis in Newtonian fluids was conducted by Chakraborty [50]. Building on this, further studies generalized this model to consider non-Newtonian effects. Relevant studies in this regard include Tripathi et al. [51] (on couple stress fluids), Channakote et al. [52] (on viscoelastic Jeffery fluids with radiative flux and wall suction effects) and Ali et al. [53] (on two fluid Ellis/Newtonian electro-osmotic peristaltic axisymmetric conduit flows). Several studies have also addressed electro-osmotic peristaltic flows of nanofluids including Tripathi et al. [54] (who examined Joule dissipation effects in finite conduits), Prakash et al. [55] (who considered magnetic body force effects in radiative-convective electro-osmotic peristaltic pumping of nanofluids) and Tripathi et al. [56] (who considered multiple peristaltic wave forms and thermal buoyancy effects). Imran et al. [57] (on Electro osmotic flow of nanofluids within a porous symmetric tapered ciliated channel). These investigations demonstrated that nanofluid properties, electro-osmotic body force and peristaltic waves can be combined to optimize pumping efficiencies in many micro-scale designs.

The Second-Grade fluid model is an important theoretical model in fluid mechanics used to describe complex, non-Newtonian fluids that exhibit viscoelastic properties. It incorporates higher-order terms into the stress-strain relationship, making it suitable for modeling fluids that exhibit both viscous and elastic behaviors. This model is particularly useful when dealing with fluids in advanced engineering, biology, and nanotechnology. The second-grade fluid model is widely used in fluid dynamics and engineering to describe complex, non-Newtonian fluid flows with both elastic and viscous characteristics. Scientific evidence from research in various fields such as polymer processing, blood flow modeling, and nanofluid studies consistently supports the use of the second-grade fluid model for accurately simulating the behavior of complex fluids. This model plays a critical role in improving the design and optimization of systems that involve non-Newtonian fluids.

Recent advancements in fractional calculus have enabled researchers to model viscoelastic fluids with more accuracy by capturing memory effects and hereditary properties inherent in such materials. A fractional second-grade fluid is an extension of the classical second-grade fluid model that incorporates fractional calculus to account for memory effects and hereditary properties of viscoelastic materials. The governing equation typically involves a fractional-order derivative, allowing for more accurate modeling of complex fluids such as biological fluids, polymeric solutions, and nanofluids. The classical second-grade model is a subclass of non-Newtonian fluids that introduces a normal stress difference, but it lacks the ability to describe long-term memory effects. The fractional second-grade model corrects this by using fractional derivatives, which better capture the time-dependent behavior and stress relaxation found in biological and engineered nanofluids. Experimental studies on blood flow and polymeric solutions have confirmed that fractional models provide a more accurate representation of real viscoelastic fluids than classical integer-order models.

The Caputo fractional derivative, in particular, provides a robust framework to describe these properties, offering insights into the time-dependent behavior of viscoelastic fluids. Despite significant progress, the combined effects of fractional derivatives, electro-osmosis, and nanofluids on peristaltic flow in ciliated geometries remain underexplored. Several important studies have been conducted in the field of peristaltic pumping of fractional second-grade fluids.

Channakote et al. [58] studied heat and mass diffusion in this context, while Abd- Alla et al. [59] focused on the effects of porous media. Channakote et al. [60] also analyzed bolus characteristics in thermal electro-osmotic analysis. Tripathi et al. [61] and Hameed et al. [62] explored hydro magnetic heat transfer during peristaltic pumping. Other significant contributions include the studies by Rathod and Mahadev [63] and Guo and Haito [64]. These studies highlight the importance of the fractional parameter in influencing flow characteristics in electro-osmotic peristaltic transport within cylindrical conduits. Tripathi and Bég [65] demonstrated that in the peristaltic pumping of fractional second-grade viscoelastic fluids through inclined conduits, the fractional parameter and Froude number increase hydrodynamic impedance, while the viscoelastic parameter, Reynolds number, inclination angle, and wave amplitude enhance flow facilitation. We examine the interaction between nanotubes and ciliated walls in electro-osmotic peristaltic flow using the elliptic beating cilia model, with heat transfer and heat generation effects, as a model of a hybrid ciliated peristaltic micro-pump for potential industrial hazardous materials applications [5] and emerging soft robotic applications [47,64,66,68].

This paper focuses on the peristaltic flow in tubes, highlighting its relevance in contemporary applications and addressing the challenges of integrating modern materials and technologies. Through this study, we aim to provide insights into the mechanisms and potential advancements that peristaltic flow can offer in cutting-edge scientific and engineering solutions. This study extends the existing literature by incorporating fractional-order derivatives for anomalous transport, ciliary motion for enhanced flow control, CNT nanofluids for improved thermal and electrical properties, and electro-osmosis in a unified peristaltic framework. These additions make it a more generalized and biologically relevant model.

The novelty of this study is attributed to its concurrent examination of ciliated walls, peristalsis, electro-osmotic body force, heat sources, thermal buoyancy, fractional viscoelastic fluid dynamics, and the incorporation of carbon nanotubes (CNTs). The analysis of physiological and biological fluids serves several key purposes.

- This study uniquely integrates fractional derivatives with the Caputo model to analyze the complex dynamics of viscoelastic nanofluids, providing new insights into electro-osmotic peristaltic streaming.
- It provides a comparative analysis of the effects of single-walled carbon nanotubes (SWCNTs) and multi-walled carbon nanotubes (MWCNTs) on the flow and thermal behavior of nanofluids.
- Fractional derivatives offer a better representation of anomalous transport behaviors, particularly in complex fluids such as CNT-based nanofluids.
- CNTs significantly enhance thermal conductivity and electro-osmotic effects, making their inclusion a notable advancement in modeling.
- The findings bridge gaps in understanding nanofluid transport in confined geometries, emphasizing applications in drug delivery, bio-inspired propulsion systems, and medical micro-pumps.

2. Mathematical formulation

In this study, we investigate electro osmosis-regulated peristaltic flow in a vertical ciliated micro-tube with a constant radius a. The fluid is an aqueous ionic nanofluid doped with carbon nanotubes (CNTs). The motion of ionic species in the fluid is induced by an external electric field applied across the electric double layer (EDL). The flow is influenced by electroosmotic and gravitational forces in a symmetric duct resembling a peristaltic micro-pump or soft robotic limb. Peristaltic pumping is generated by sinusoidal waves along the tube walls with a constant wave speed c and wavelength λ. The physical model is illustrated in Fig. 1 with a static electric field applied. The cylindrical coordinate system (r, z, t) is used for mathematical analysis of the flow phenomena.

This study is based on specific assumptions that also serve as limitations.

- The fractional viscoelastic second-grade Reiner-Rivlin differential model is used to study rheological effects.
- A nanofluid is created by suspending carbon nanotubes in a base fluid.
- An external electric field with a constant strength E_z is applied to blood flow in the positive z-direction to induce electro-osmotic force.
- Caputo's fractional derivative is employed to model viscoelastic memory effects, crucial for capturing the time-dependent stress-strain behavior of biological fluids.
- The Debye–Hückel hypothesis simplifies the Poisson–Boltzmann equation for a more accurate calculation of the electric potential in the electric double layer. However, this simplification may neglect important nonlinear dynamics in real-world situations.
- The channel walls are maintained at a constant temperature T_0.

The fractional-order derivative according to Caputo's is defined

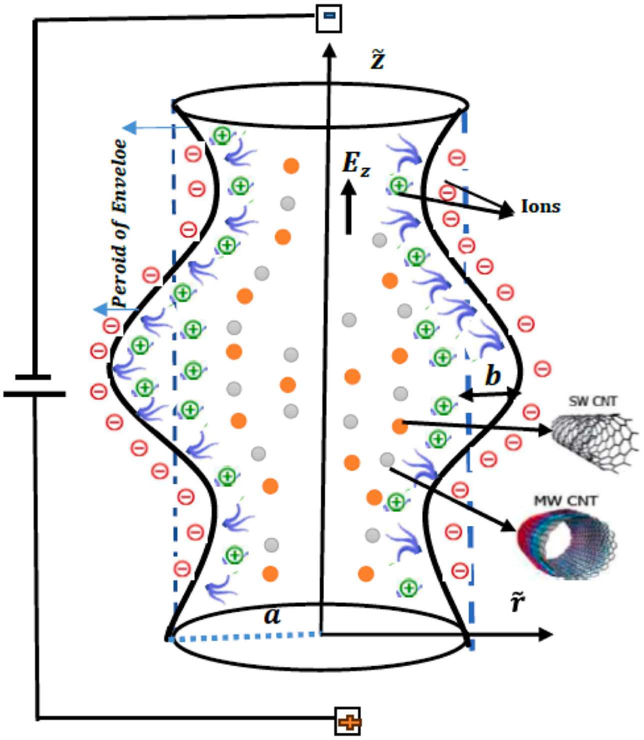

Fig. 1. Physical model.

following Tripathi and Bég [61] as:

$$D^{\alpha^*} f(t) = \frac{1}{\Gamma(n-\alpha^*)}\int_b^t \frac{f^n(\tau)}{(t-\tau)^{\alpha^*+1-n}}\, d\tau\,(n-1 < Re(\alpha^*) \le n,\ n \in N), \tag{1}$$

Let n be a natural number, and $R_e(\alpha^*) \le n$, where α^* represents the order of the derivative and can be real or complex. Let b be the initial value of the function f. For Caputo's derivative, we have:

$$D^{\alpha^*} t^{\beta_1} = \begin{cases} 0 \ if\ (\beta_1 \le \alpha^* - 1) \\ \dfrac{\Gamma(\beta_1+1)}{\Gamma(\beta_1-\alpha^*+1)} t^{\beta_1-\alpha^*}\ if\ (\beta_1 > \alpha^* - 1). \end{cases} \tag{2}$$

The equation for a fractional second-grade liquid with the fractional model is:

$$\widetilde{S} = \mu\left(1 + \widetilde{\lambda}_1^{\alpha_1}\frac{\partial^{\alpha_1}}{\partial \widetilde{t}^{\alpha_1}}\right)\dot{\gamma}, \tag{3}$$

The shear stress is denoted by $\widetilde{S}$, the material parameter by $\widetilde{\lambda}_1$, the time by $\widetilde{t}$, the dynamic viscosity by μ, the shear strain rate by $\dot{\gamma}$, and the fractional parameter by α_1 such that $(0 < \alpha_1 \le 1)$. The model simplifies to the traditional second-grade model when $\alpha_1 = 0$, and the classical Newtonian (Navier-Stokes) case occurs when $\widetilde{\lambda}_1 = 0$.

The metachronal motion of the cilia tip envelops on the inner surfaces of the cylindrical micro-tube wall is simulated, following Ramesh et al. [39] by the following expressions:

The distensible micro-tube wall contracts and relaxes, and the compliant motion can be mathematically expressed as follows:

$$\widetilde{h} = a + b\cos[2\pi(\widetilde{Z} - c\widetilde{t})] \tag{4}$$

$$\widetilde{R} = \widetilde{H} = f(\widetilde{Z},\ \widetilde{t}) = a + a\ \epsilon\cos\left(\frac{2\pi}{\widetilde{\lambda}}(\widetilde{Z} - c\ \widetilde{t})\right), \tag{5a}$$

$$\widetilde{Z} = \widetilde{g}(\widetilde{Z}, \widetilde{Z}_0, \widetilde{t}) = a + \ a\ \epsilon\alpha\ \sin\ \left(\frac{2\pi}{\widetilde{\lambda}}(\widetilde{Z} - c\ \widetilde{t})\right), \tag{5b}$$

Here a represents the mean radius of the tube, ϵ is a non- dimensional measure with respect to the cilia length, and $\widetilde{\lambda}$ is the wavelength of the metachronal wave, c is the wave speed, $\widetilde{Z}_0$ is the reference position of the particle and α is the measure of the eccentricity of the elliptical motion. The cilia are evenly spaced and extend from both walls of the infinite channel. A metachronal wave is created by the natural movement of the cilia, propagating parallel to the fluid flow.

The cilia are arranged at equal intervals and protrude normally from both walls of the infinitely long channel. A metachronal wave is generated due to natural beating of cilia and the direction of wave propagation is parallel to the direction of fluid flow. The governing equations for mass, momentum and energy (heat) conservation are developed by generalizing previous studies [40,41,60,64,65] to include heat source, electro-osmotic body force, fractional second grade visco-elastic and thermal convection effects as follows:

$$\frac{\partial\widetilde{U}}{\partial\widetilde{R}} + \frac{\widetilde{U}}{\widetilde{R}}\frac{\partial\widetilde{W}}{\partial\widetilde{R}} = 0, \tag{6}$$

$$\begin{aligned}\rho_{nf}\left(\frac{\partial\widetilde{U}}{\partial\widetilde{t}} + \widetilde{U}\frac{\partial\widetilde{U}}{\partial\widetilde{R}} + \widetilde{W}\frac{\partial\widetilde{U}}{\partial\widetilde{Z}}\right) = &-\frac{\partial\widetilde{p}}{\partial\widetilde{R}} \\ &+ \mu_{nf}\left(1 + \widetilde{\lambda}_1^{\alpha_1}\frac{\partial^{\alpha_1}}{\partial\widetilde{t}^{\alpha_1}}\right)\left[\frac{1}{\widetilde{R}}\frac{\partial}{\partial\widetilde{R}}\left(\widetilde{R}\frac{\partial\widetilde{U}}{\partial\widetilde{R}}\right) + \frac{\partial^2\widetilde{U}}{\partial\widetilde{Z}^2}\right] \\ &+ \rho_e E_R\end{aligned} \tag{7}$$

$$\begin{aligned}\rho_{nf}\left(\frac{\partial\widetilde{W}}{\partial\widetilde{t}} + \widetilde{U}\frac{\partial\widetilde{W}}{\partial\widetilde{R}} + \widetilde{W}\frac{\partial\widetilde{W}}{\partial\widetilde{Z}}\right) = &-\frac{\partial\widetilde{p}}{\partial\widetilde{Z}} \\ &+ \mu_{nf}\left(1 + \widetilde{\lambda}_1^{\alpha_1}\frac{\partial^{\alpha_1}}{\partial\widetilde{t}^{\alpha_1}}\right)\left[\frac{1}{\widetilde{R}}\frac{\partial}{\partial\widetilde{R}}\left(\widetilde{R}\frac{\partial\widetilde{W}}{\partial\widetilde{R}}\right) + \frac{\partial^2\widetilde{W}}{\partial\widetilde{Z}^2}\right] \\ &+ (\rho\gamma)_{nf}(\widetilde{T} - T_0)g + \rho_e E_z\end{aligned} \tag{8}$$

$$(\rho c_p)_{nf}\left(\frac{\partial\widetilde{T}}{\partial\widetilde{t}} + \widetilde{U}\frac{\partial\widetilde{T}}{\partial\widetilde{R}} + \widetilde{w}\frac{\partial\widetilde{T}}{\partial\widetilde{Z}}\right) = k_{nf}\left(\frac{\partial^2\widetilde{T}}{\partial\widetilde{R}^2} + \frac{1}{\widetilde{R}}\frac{\partial\widetilde{T}}{\partial\widetilde{R}} + \frac{\partial^2\widetilde{T}}{\partial\widetilde{Z}^2}\right) + \widetilde{Q}_0, \tag{9}$$

In the context of Eqs. (6)–(9), $\widetilde{U}$ and $\widetilde{W}$ denote the velocity components in the radial and axial directions, respectively. E_R and E_z represent the electric body forces in the radial and axial coordinates.

In eqn. (7) the terms on the left relate to unsteady and convective acceleration, the first term on the right is the radial pressure gradient, the next terms are the modified fractional viscoelastic terms and the final term on the right is the radial electro-osmotic body force. In qn. (8), the terms on the left relate again to unsteady and convective acceleration, the first term on the right is the axial pressure gradient, the next terms are the modified fractional viscoelastic terms, the penultimate term is thermal buoyancy and the final term on the right is the axial electro-osmotic body force. In the energy eqn. (9) the first term on the left is the transient temperature term, followed by the convective thermal terms. On the right-hand side, the first terms are thermal diffusion (based on the Fourier heat conduction law) and the final term is heat generation/absorption.

When the no-slip boundary condition is applied, the velocity components of the CNT-ionic nanofluid are influenced by the motion of cilia tips, which can be mathematically expressed accordingly.

$$\widetilde{W} = \left(\frac{\partial\widetilde{Z}}{\partial\widetilde{t}}\right)_{\widetilde{Z}_0} = \frac{\partial\widetilde{g}}{\partial\widetilde{t}} + \frac{\partial\widetilde{g}}{\partial\widetilde{Z}}\frac{\partial\widetilde{Z}}{\partial\widetilde{t}} = \frac{\partial\widetilde{g}}{\partial\widetilde{t}} + \frac{\partial\widetilde{g}}{\partial\widetilde{Z}}\widetilde{W}, \tag{10}$$

$$\widetilde{U}=\left(\frac{\partial\overline{R}}{\partial\overline{t}}\right)_{\tilde{z}_0}=\frac{\partial\overline{f}}{\partial\overline{t}}+\frac{\partial\overline{f}}{\partial\overline{Z}}\frac{\partial\overline{Z}}{\partial\overline{t}}=\frac{\partial\widetilde{f}}{\partial\overline{t}}+\frac{\partial\widetilde{f}}{\partial\widetilde{z}}\widetilde{W}. \tag{11}$$

Equations. (5a, b) when implemented in Eqns. (10) and (11), yield:

$$\widetilde{W}=\frac{-\frac{2\pi}{\lambda}\left(\epsilon\alpha a\cos\left(\frac{2\pi}{\lambda}\right)(\overline{Z}-c\overline{t})\right)}{1-\frac{2\pi}{\lambda}\left(\epsilon\alpha a\cos\left(\frac{2\pi}{\lambda}\right)(\overline{Z}-c\overline{t})\right)}, \tag{12}$$

$$\widetilde{U}=\frac{\frac{2\pi}{\lambda}\left(\epsilon ac\sin\left(\frac{2\pi}{\lambda}\right)(\overline{Z}-c\overline{t})\right)}{1-\frac{2\pi}{\lambda}\left(\epsilon\alpha a\cos\left(\frac{2\pi}{\lambda}\right)(\overline{Z}-c\overline{t})\right)}, \tag{13}$$

The effective density ρ_{nf}, specific heat $(cp)_{nf}$ and thermal expansion coefficient α_{nf} of the CNT-aqueous ionic nanofluid are determined using the general mixing rule. Subsequently, the viscosity μ_{nf} and thermal conductivity k_{nf} of the nanofluid are calculated using the Maxwell model and Brinkman's relations, which are given respectively as follows:

$$\left.\begin{array}{c}\rho_{nf}=(1-\phi)\rho_f+\phi\rho_{CNT},\ \mu_{nf}=\dfrac{\mu_f}{(1-\phi)^{2.5}}\\ (\rho c_p)_{nf}=(1-\phi)(\rho c_p)_f+\phi(\rho c_p)_f,\ \alpha_{nf}=\dfrac{k_{nf}}{(\rho c_p)_{nf}}\\ (\rho\gamma)_{nf}=(1-\phi)(\rho\gamma)_f+\phi(\rho\gamma)_{CNT},\\ k_{nf}=k_f\left(\dfrac{(1-\phi)+\dfrac{2\phi k_{CNT}}{k_{CNT}-k_f}\log\left(\dfrac{k_{CNT}+k_f}{2k_f}\right)}{(1-\phi)+\dfrac{2\phi k_f}{k_{CNT}-k_f}\log\left(\dfrac{k_{CNT}+k_f}{2k_f}\right)}\right)\end{array}\right\}, \tag{14}$$

Here ϕ represents the volume fraction of carbon nanotubes (CNTs), subscript f represents the properties of the base fluid and superscript p represents the solid particle properties.

The Poisson–Boltzmann equation describes the distribution of the electric potential in the aqueous ionic nanofluid as follows:

$$\nabla^2\widetilde{\Phi}=\frac{1}{\widetilde{R}}\frac{\partial}{\partial\widetilde{R}}\left(\widetilde{R}\frac{\partial\widetilde{\Phi}}{\partial\widetilde{R}}\right)=\frac{\rho_e}{\varepsilon_r\varepsilon_0}. \tag{15}$$

Here, ∇^2 is the Laplacian operator, Φ is the electric potential, ρ_e is the charge density, and ε_r is the relative permittivity of the medium, ε_0 denotes the permittivity of the vacuum, and the electric number density in terms of the number cations n^+ and the anions n^- is described as follows:

$$\rho_e=ez(n^+-n^-). \tag{16}$$

In order to analyze the fluid dynamics of the peristaltic moving boundary problem in a steady state, it is essential to convert the coordinates from the laboratory frame $(\widetilde{Z},\widetilde{R})$ to a wave frame of reference(r, z). The transformation equations for the coordinates can be expressed as follows:

$$\widetilde{r}=\overline{R},\widetilde{z}=\widetilde{Z}-c\widetilde{t},\ \widetilde{u}=\widetilde{U},\ \widetilde{w}=\widetilde{W}-c,\widetilde{p}(\widetilde{z},\widetilde{r},\widetilde{t})=\widetilde{p}(\widetilde{Z},\widetilde{R},\widetilde{T}). \tag{17}$$

The flow problem under consideration can be effectively simplified through the application of non-dimensional analysis. This involves introducing dimensionless scaling variables which are Sadaf and Nadeem [34] and Iqra et al., [35] defined as follows:

$$\left.\begin{array}{l}m=\sqrt{\dfrac{2n_0\,e^2z^2a^2}{\varepsilon_0\varepsilon_rk_f\widetilde{T}_{avg}}}=\dfrac{a}{\lambda_d},U_{hs}=\dfrac{E_z\varepsilon_r\,k_f\widetilde{T}_{avg}\varepsilon_0}{ez\mu_fc},\ p=\dfrac{a^2\widetilde{p}}{c\lambda\,\mu_f},\ \theta=\dfrac{\widetilde{T}-T_0}{T_0},\ t=\dfrac{c\widetilde{t}}{\lambda},\\ B=\dfrac{Q_0d^2}{T_0k_f},\ \Phi=\dfrac{ez\widetilde{\Phi}}{k_fT_{avg}},w=\dfrac{\widetilde{w}}{c},\ W=\dfrac{\widetilde{W}}{c}\ u=\dfrac{\widetilde{U}}{c\delta},\ z=\dfrac{\widetilde{Z}}{\lambda},Z=\dfrac{\widetilde{Z}}{\lambda},R=\dfrac{\widetilde{R}}{a},\ r=\dfrac{\widetilde{r}}{a},\\ L=\dfrac{(\rho\gamma)_{nf}}{(\rho\gamma)_f},\ Re=\dfrac{\rho_f\,c\,a}{\mu_f},u=\dfrac{\lambda\widetilde{u}}{ac},\delta=\dfrac{a}{\lambda},\epsilon=\dfrac{b}{a},\ h=\dfrac{\widetilde{h}}{a},\mathrm{Pr}=\dfrac{c_p\mu_f}{k_f},\lambda_1^{\alpha_1}=\dfrac{c\widetilde{\lambda^{\alpha_1}}_1}{\lambda},\\ Gr=\dfrac{(\rho\gamma)_fga^2T_0}{\mu_fc},\end{array}\right\} \tag{18}$$

Next, employing the lubrication linearization theory for long wavelengths and low Reynolds numbers, we arrive at the following simplified equations:

$$\frac{1}{r}\frac{\partial(r\,w)}{\partial r}+\frac{\partial u}{\partial z}=0, \tag{19}$$

$$\frac{\partial p}{\partial r}=0, \tag{20}$$

$$\frac{\partial p}{\partial z}=\left(1+\lambda_1^{\alpha_1}\frac{\partial^{\alpha_1}}{\partial t^{\alpha_1}}\right)\frac{\mu_{nf}}{\mu_f}\left\{\frac{1}{r}\frac{\partial}{\partial r}\left(r\frac{\partial w}{\partial r}\right)\right\}+GrL\,\theta+\frac{1}{r}\frac{\partial}{\partial r}\left(r\left(\frac{\partial\Phi}{\partial r}\right)\right)U_{hs}, \tag{21}$$

$$\frac{1}{r}\frac{\partial}{\partial r}\left(r\frac{\partial\theta}{\partial r}\right)+B\left(\frac{k_f}{k_{n_f}}\right)=0, \tag{22}$$

$$\frac{1}{r}\frac{\partial}{\partial r}\left(r\frac{\partial\Phi}{\partial r}\right)=m^2\left(\frac{\mathrm{n}^+-\mathrm{n}^-}{2}\right). \tag{23}$$

Here U_{hs} designate the electro-osmotic Helmholtz-Smoluchowski velocity, B is the dimensionless heat source parameter, Gr is the Grashof number, m is the electro-osmotic Debye–Hückel parameter, θ is the dimensionless temperature parameter, λ_1 is second grade viscoelastic material parameter, (ϕ) is carbon nanotube (CNT) volume fraction and the cilia length parameter is denoted by (β). The linearized Boltzmann distribution is suitable for estimating the electric potential in a fluid medium when the zeta potential is low. This method provides an accurate assessment of the local ionic distribution of ionic species without introducing additional complexity to the flow problem. The resulting electric potential, similar to the majority of electrolyte solutions, typically falls within the range of less than or equal to 25 mV.

$$n^{\pm}=e^{\mp\Phi}. \tag{24}$$

Using Eq. (24) in Eq. (21) we get the Poisson–Boltzmann equation, following Tripathi et al. [51] as follows:

$$\frac{1}{r}\frac{\partial}{\partial r}\left(r\frac{\partial\Phi}{\partial r}\right)=m^2\sinh(\Phi)\ . \tag{25}$$

With the use of the Debye–Hückel approximation, as proposed by Tripathi et al. [51],

Eq. (25) is further reduced, using the approximation that $\sinh(\Phi)\cong\Phi$, to:

$$\frac{1}{r}\frac{\partial}{\partial r}\left(r\frac{\partial\Phi}{\partial r}\right)=m^2\Phi. \tag{26}$$

In the wave frame, the suitable boundary conditions are defined by the following equations as proposed by Butt et al. [40] and Hanasoge et al. [42]:

$$\frac{\partial w}{\partial r}=0\ at\ r=0,\ w=\frac{-2\pi\ \epsilon\alpha\ \beta\cos(2\pi z)}{1-2\pi\ \epsilon\ \alpha\ \beta\cos(2\pi z)}-1\ at\ r=h, \tag{27}$$

$$\frac{\partial\theta}{\partial r} = 0 \ at \ r = 0, \ \theta = 0, \ h = 1 + \epsilon\cos(2\pi z), \tag{28}$$

$$\frac{\partial\Phi}{\partial r} = 0 \quad \text{at} \quad r = 0 \quad \text{and} \quad \Phi = 1 \quad \text{at} \quad r = h(z). \tag{29}$$

3. Analytical solutions

By applying the boundary conditions from Eq. (29) to solve Eq. (26), we derive the electrical potential function as:

$$\Phi = \frac{I_0(m\ r)}{I_0(m\ h)} \tag{30}$$

Here I_0 is a Bessel's function. The exact solutions to Eqns. (21) and (22), satisfying the boundary conditions (27) and (28), emerge as:

$$w = \frac{1}{2\pi\alpha\beta\epsilon\cos(2\pi z) - 1} + \frac{\mu f\left(\frac{(h^2 - r^2)\left(-16k_{nf}\frac{dp}{dz} + BGrk_f L(3h^2 - r^2)\right)}{k_{nf}} + 64\left(-1 + \frac{I_0\ (m\ r)}{I_0\ (m\ h)}\right)U_{hs}\right)}{64A_1\mu_{nf}}. \tag{31}$$

The solution of temperature is as follows:

$$\theta = \frac{B\ k_f}{4k_{nf}}(h^2 - r^2). \tag{32}$$

To calculate the pressure gradient, we use the volumetric flow rate in the moving frame, resulting in the following equation:

$Q = 2\int_0^h r\ w\ dr$, in consequences as a result of Eqn. (31), becomes:

$$Q = \frac{\left(B\ Gr\ h^6\ k_f\ L - 6h^4 k_{nf}\frac{dp}{dz}\right)\mu_f}{48k_{nf}A_1\mu_{nf}} + \frac{h^2}{2\pi\alpha\beta\epsilon\cos(2\pi z) - 1} + \frac{h^2\ \mu_f \mathrm{I}_2(hm)U_{hs}}{A_1\mu_{nf}\mathrm{I}_0(hm)}. \tag{33}$$

The time-averaged flow rate Q is then computed as:

$$\widetilde{Q} = Q + \frac{1}{2}\left(1 + \frac{\epsilon^2}{2}\right). \tag{34}$$

Eq. (33) as a result of Eq. (34) takes the form:

$$\frac{dp}{dz} = -\frac{8A_1\mu_{nf}\left(Q - A_2 - \frac{h^2}{2\pi\alpha\beta\epsilon\cos(2\pi z) - 1} - A_3\right)}{h^4\ \mu_f}. \tag{35}$$

Where,

$$A_1 = \left(1 + \lambda_1^{\alpha_1}\left(\frac{t^{\alpha_1}}{\Gamma(1 - \alpha_1)}\right)\right),$$

$$A_2 = \frac{\mathrm{BGr}h^6 k_f L\mu_f}{48k_{nf}A_1\mu_{nf}},$$

$$A_3 = \frac{h^2\mu_f\ \mathrm{I}_2(h\ m)U_{hs}}{A_1\mu_{nf}\mathrm{I}_0(h\ m)}.$$

The pressure rise Δp and friction force F_λ are, respectively, given by

$$\Delta p = \int_0^1 \frac{\partial p}{\partial z}dz, \tag{36}$$

$$F_\lambda = \int_0^1 \left(-h^2\frac{\partial p}{\partial z}\right)dz. \tag{37}$$

The expression for resultant stream function can be obtained by the following equations:

$w = -\frac{1}{r}\frac{\partial\psi}{\partial z},\ w = \frac{1}{r}\frac{\partial\psi}{\partial r}\ at\ r = h$. (38)

4. Results and discussion

Here, we have discussed the graphical representation of physical quantities for various senarios. We have provided detailed explanations for the trends in axial velocity, temperature, pressure gradient, pressure rise, and streamlines.

Fig. 2 and Table 1 show data on the effective thermal conductivity of nanofluids with single-walled carbon nanotubes (*SWCNT*) and multi-walled carbon nanotubes (*MWCNT*).

Notably, *MWCNT* exhibits a higher thermal conductivity compared to *SWCNT*. Furthermore, the difference between *SWCNT* and *MWCNT* becomes more pronounced as the volume fraction in the nanofluid increases ($\phi > 0$). Next, we address the impact of key multi-physics parameters on velocity, temperature, axial pressure gradient, and pumping and trapping characteristics for the regime. **Mathematica** software has been utilized to compute analytical solutions and represented as graphs with physically viable data.

4.1. Velocity profiles

The axial velocity distribution for various Helmholtz-Smoluchowski velocity parameter is illustrated in Fig. 3(a). It is observed that an increase in positive U_{hs} velocity leads to an increase in axial velocity for both SWCNT/water and MWCNT/water ionic nanofluids in the core

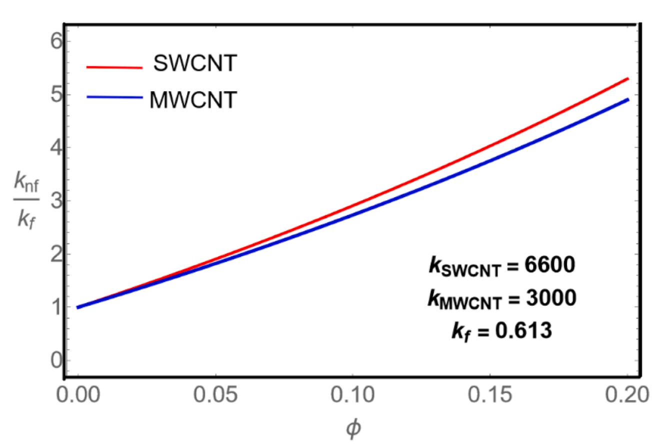

Fig. 2. The efficient thermal conductivity of the nanofluid.

Table 1
The thermal characteristics of the base fluid, specifically water, and carbon nanotubes [48].

Fluid phase (water)		Cu	SWCNT	MWCNT
c_p	4179	385	425	796
ρ	997.1	8933	2600	1600
k	0.613	400	6600	3000

zone of the micro-tube (around the centerline $r = 0$) whereas a clear deceleration is encountered in the peripheral zone i.e. near the boundaries of the tube($r = 1, -1$). The Helmholtz-Smoluchowski parameter, as defined in eqn. (18) as $U_{hs} = \frac{E_z\varepsilon_r\ k_f\widetilde{T}_{avg}\varepsilon_0}{ez\mu_f c}$ and is directly proportional to the axial electrical field, E_Z. This parameter features in the electro-osmotic body force, $\frac{1}{r}\frac{\partial}{\partial r}\left(r\left(\frac{\partial\Phi}{\partial r}\right)\right)U_{hs,}$ in the dimensionless axial momentum conservation Eqn. (21). For positive values of U_{hs} the body force is assistive, and this induces acceleration in the core region. However, since the micro-tube has a closed boundary, conservation of momentum

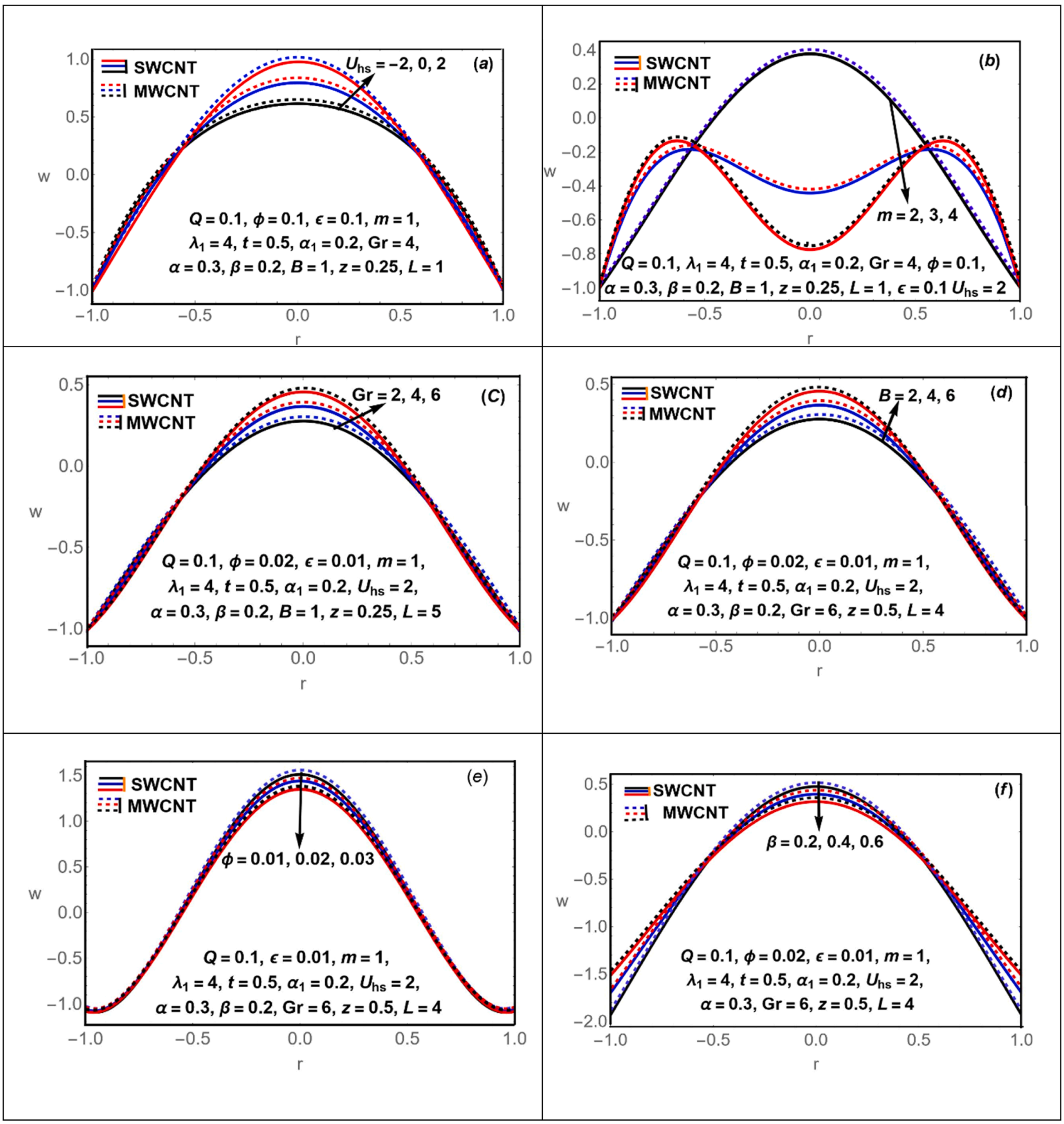

Fig. 3. Axial velocity distribution with variation in (a) Helmholtz-Smoluchowski velocity parameter (U_{hs}), (b) electro-osmotic parameter (m),(c) Grashof number (Gr), (d) Thermal source/sink parameter (B), (e) carbon nanotube (CNT) volume fraction (ϕ). (f) Cilia parameter (β).

leads to a deceleration in the peripheral zones. This trend has been observed in many other studies of electro-kinetic peristalsis including Chakraborty [50] where electrical field is shown to modulate beneficially the axial flow and therefore enhance volumetric flow rate. However, when negative values of U_{hs} are prescribed this corresponds to a reversal in the direction of axial electrical field, E_z and the electro-osmotic body force becomes opposing which leads to a strong retardation in the core flow. As a result, a slight flow acceleration is produced in the peripheral zones near the boundaries. Reverse electrical field can therefore be utilized to modulate the peristaltic axial flow whereas aligned (positive) electrical field can be deployed to accelerate the flow. *MWCNTs* clearly attain a slightly greater axial velocity at all locations across the micro-tube cross-section relative to *SWCNTs*. The impact of the electro-osmotic parameter (m) on the axial velocity profile is depicted in Fig. 3(b). It is observed that an increase in the electro-osmotic parameter, m, corresponding to a smaller Debye length, results in a significant deceleration at the center of the micro-tube. For $m = 2, 3$ the core profile (topology) is parabolic, and the trend is consistent deceleration across the micro-tube i.e. for all radial locations; however, at the largest value of $m = 4$ the profile becomes an inverted parabola in the essential zone while deceleration still arises in the core zone, there is an accompanying minor axial flow speeding up in the peripheral zone which is absent for the other two smaller values of m. This indicates that a critical m value exists where axial flow response is modified in the micro-tube and after which the response in axial velocity is not consistent across the span of the micro-tube. The parameter, $m = \sqrt{\frac{2n_0 \ e^2 \underset{\sim}{z}^2 a^2}{\varepsilon_0 \varepsilon_r k_f T_{avg}}}$ features in the reduced electrical potential eqn. (26), in the term, $m^2\Phi_{.}$. It does not explicitly arise in the axial momentum eqn. (21), however via the electrical potential coupling with the electro-osmotic body force term in eqn. (21), $\frac{1}{r}\frac{\partial}{\partial r}\left(r\left(\frac{\partial \Phi}{\partial r}\right)\right)U_{hs,}$ a significant indirect influence is exerted on the axial velocity field. The parameter m as noted is inversely related to the electric double layer (EDL).

As m is increased a thinner EDL is produced and for smaller m the EDL is much thicker. This influences the ionic distribution and electrical potential generated at the boundaries which in turn modifies the velocity field. This pattern of behavior concurs with earlier studies including Guo and Haitao [64], among others. Again, marginally greater axial velocity magnitudes are observed for *MWCNTs* as compared to *SWCNTs*. Very close to the boundaries, flow reversal (backflow) is observed in both Fig. 3a and b, indicated by the negative velocities observed in these locations. Effectively both electrical potential and axial electrical field can be utilized to manipulate the axial flow distribution in micro-tube peristaltic propulsion and both these mechanisms are non-intrusive, offering significant control advantages in microfluidic device design. Fig. 3(c) illustrates the response of axial fluid velocity (w) with (Gr). It is observed that across the entire span of the micro-tube, particularly in the core (middle) region, the velocity profile consistently increases with rising thermal Grashof number for both SWCNT/water and MWCNT/water nanofluids. A higher Gr value signifies a stronger thermal buoyancy effect compared to viscous force. The thermal buoyancy body force, $GrL\ \theta$ in Eqn. (21) is amplified and this mobilizes strong natural convection currents which intensify and accelerate the flow. For the case $Gr = 0$, thermal buoyancy vanishes and forced convection is present (de-coupling of momentum Eq. (21) with energy Eq. (22)). Fig. 3(d) visualizes the impact of heat source parameter, B on velocity distribution across the micro-tube radial span. A substantial enhancement in axial velocity in the core zone accompanies an increase in heat generation (positive B). The addition of thermal energy to the ciliated peristaltic regime energizes the flow via the $B\left(\frac{k_f}{k_{n_f}}\right)$ term in the energy eqn. (22). The heat generation may be associated with a thermal hot spot in the peristaltic micro-pump which can act as a source for heat injection into the regime. However, the core zone is accelerated strongly via momentum re-distribution; the peripheral zone near the micro-tube walls experiences a deceleration. The impact on velocity distribution for different values of CNT volume fraction ϕ is presented in Fig. 3(e). The velocity of SWCNT/water and MWCNT/water nanofluids notably decrease as ϕ increases. As the volume fraction of CNTs (ϕ) increases, the fluid becomes more viscous and experiences higher internal resistance (drag), leading to a noticeable reduction in the velocity of both SWCNT/water and MWCNT/water nanofluids. This effect is crucial for applications where controlling fluid flow or enhancing thermal properties are key, such as in biomedical or cooling systems. MWCNTs are slightly more effective than SWCNTs in this regard. Fig. 3(f) shows the impact of cilia slenderness parameter, β, on axial flow. Both cilia spacing and length influence the viscous resistance experienced by each cilium, affecting the axial flow. Longer cilia hinder axial flow, especially in the core region, altering the pressure gradient and energy distribution within the system governed by synchronized cilia beating along the microtube's inner surfaces. When $\beta = 0$, (not plotted) indicating no cilia and metachronal wave activity, flow is driven solely by peristaltic action due to wall flexibility. Longer cilia restrict axial flow in the core region but accelerate flow in peripheral areas near the walls where cilia influence is more significant. However, excessive cilia length can have adverse effects in the core zone. Previous studies by Blake [37] and Manzoor et al. [45], support this observation, particularly for viscoelastic fluids. Determining a critical cilia length can optimize core flow in conjunction with peristaltic wave motion. Moreover, multi-walled carbon nanotubes (*MWCNTs*) exhibit slightly higher axial velocity magnitudes than single-walled carbon nanotubes (*SWCNTs*) in the micro-tube. Overall, Fig. 3 demonstrates that axial flow may be optimized, at least in the core zone of the micro-tube, with smaller cilia length, positive aligned axial electrical field, strong heat source, higher CNT volume fraction and maximum thermal buoyancy effect (high Grashof number).

4.2. Temperature profiles

The impact of the heat source/sink parameter, denoted as B and the CNT volume fraction, ϕ, on the temperature profiles across the micro tube are visualized in Fig. 4(a) and (b). The influence of the heat source parameter on the temperature distribution is clearly illustrated in Fig. 4 (a). The temperature profile exhibits an increasing trend with higher values of the heat source parameter (B) across all radial positions. The injection of thermal energy significantly enhances temperature levels within the ciliated peristaltic flow regime. Although the heat sink scenario $(B < 0)$ has not been depicted, it would induce the opposite effect, leading to cooling throughout both the core and peripheral regions of the microtube.

In contrast, an increase in the CNT volume fraction (ϕ) results in a reduction in temperature across the domain. This phenomenon arises due to the high thermal conductivity of CNTs, which facilitates rapid heat dissipation toward the channel walls. Consequently, the fluid temperature experiences a sharp decline as the thermal energy generated by the heat source is efficiently conducted away. This characteristic underscores the suitability of CNTs in applications requiring effective heat removal, such as thermal regulation in micro-peristaltic ciliated pumps used for hazardous waste transport [5] and temperature control in soft robotic limbs [67]. The observed thermal behavior aligns well with trends reported in previous studies [44].

4.3. Axial pressure gradients

In peristaltic flow, a controlled pressure gradient is essential for directing fluid movement within tubes or biological conduits. Muscle contractions create a unidirectional wave-like motion, preventing backflow. The pressure gradient magnitude and peristaltic wave frequency and amplitude influence flow rate, allowing precise control by

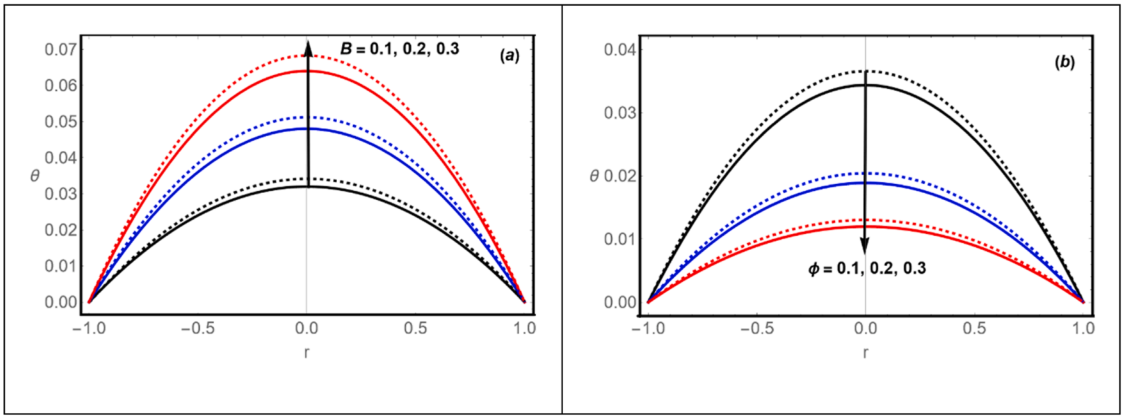

Fig. 4. (a) Impact of B on θ Fig. 4(b) Impact of ϕ on θ
[For fixed values of other parameters($\phi = 0.11, \epsilon = 0.1, z = 0.5$)].

adjusting muscle (or artificial wall) contractions. In biological systems, peristaltic flow efficiently transports substances, and understanding and manipulating the pressure gradient are crucial in applications such as medical devices, industrial micro-pumps *etc.* in order to achieve optimized fluid transport. The pressure gradient for different values of m and U_{hs}, and at different axial coordinate (z), are plotted in Fig. 5a–d. Fig. 5(a) illustrates the relationship between the pressure gradient and the inverse thickness of the electrical double layer (EDL), characterized by the Debye–Hückel parameter, $(a/\lambda d)$. The results demonstrate that as m increases, the pressure gradient also rises. Physically, this implies that when the characteristic thickness of the EDL decreases (i.e., when the electrostatic screening length λd becomes smaller relative to the characteristic length scale a), the system exhibits a stronger tendency toward a negative pressure gradient. This phenomenon can be understood in terms of electrostatic interactions and fluid dynamics. A thinner EDL corresponds to a higher charge density near the surface, leading to stronger electrostatic forces that influence the flow characteristics within the system. As the EDL becomes more compact, the interplay between electrostatic forces and hydrodynamic effects intensifies, which in turn alters the pressure distribution. The increasing magnitude of the negative pressure gradient suggests that the fluid experiences greater resistance or suction effects due to the enhanced electrostatic forces, which could impact flow stability and overall transport properties within the system. In Fig. 5(b), it is evident that an increase in the Helmholtz-Smoluchowski velocity (U_{hs}), which scales proportionally with the applied axial electric field, enhances the electroosmotic flow. This, in turn, results in a steady increase in the pressure gradient along the channel. Physically, this occurs because the externally applied electric field exerts a stronger electrokinetic force on the charged fluid near the channel walls, inducing greater fluid motion. Additionally, as the electric field intensity rises, it counteracts adverse pressure gradients that would otherwise lead to flow reversal or instability. This stabilizing effect reduces the likelihood of localized backflows and ensures smoother fluid transport under such conditions. The influence of electro-osmotic parameters-such as the inverse electric double-layer (EDL) parameter (m) and the Helmholtz-Smoluchowski velocity (U_{hs})-remains uniform across all axial positions (z − values), indicating a sustained interaction between electrokinetic forces and the fluid motion. Additionally, a comparison between multi-walled carbon nanotubes (*MWCNT*) and single-walled carbon nanotubes (*SWCNT*) reveals that (*MWCNT*) based nanofluids exhibit a slightly higher-pressure gradient. This difference is likely due to the increased thermal conductivity and surface interactions of (MWCNTs), which enhance heat transfer and modify the fluid's rheological properties, thereby influencing the overall pressure distribution within the microtube.

Fig. 5(c) and (d) illustrate the variation of the axial pressure gradient for diverse values of the thermal Grashof number (Gr) and the heat generation parameter (B). These figures clearly indicate that an increase in either Gr or B results in a corresponding rise in the pressure gradient. This behavior can be understood through the combined effects of thermal buoyancy and internal heat generation, both of which enhance the driving force for fluid motion. From a physical standpoint, the thermal Gasthof number (Gr) quantifies the influence of buoyancy forces relative to viscous forces in a thermally driven flow. Buoyancy effects arise due to temperature-induced density variations within the fluid. When the temperature of the fluid near a heated surface increase, thermal expansion reduces its density, making it lighter relative to the surrounding cooler fluid. This density difference creates an upward buoyant force that promotes convective motion. As Gr increases, the strength of this buoyant force grows, thereby intensifying fluid movement and leading to a steeper pressure gradient. Similarly, the heat generation parameter (B) accounts for internal energy sources within the fluid, which further modify the thermal environment. Internal heat generation could stem from various physical mechanisms, such as exothermic chemical reactions, viscous dissipation, or radiative heating. When (B) increases, additional heat is introduced into the system, further elevating the fluid temperature. This localized heating reinforces thermal buoyancy by amplifying temperature gradients, which in turn enhances the upward motion of the fluid. The combined effect of stronger buoyancy and increased internal energy leads to a more pronounced pressure gradient, as the fluid experiences greater thermal forcing that drives its movement. Thus, the observed increase in the pressure gradient with higher Gr and B values can be attributed to the strengthening of convective transport mechanisms, where thermal energy contributes to dynamic pressure variations that influence the overall flow characteristics within the system. These combined effects enhance the axial pressure gradient, leading to an increase in flow momentum throughout the microchannel. The pressure gradient reaches its maximum at the midpoint of the microtube $(z = 0.5)$, suggesting that the flow experiences the highest hydrodynamic resistance at this location due to the competing effects of peristaltic motion, electro-osmosis, and ciliary propulsion. In contrast, near the inlet $(z = 0)$ and outlet $(z = 1)$, the pressure gradient is lower, implying a gradual acceleration of the fluid as it moves toward the center, where resistance is highest, followed by a deceleration as it exits the channel. This behavior is characteristic of pressure-driven microchannel flows, where the balance between viscous forces, electrokinetic effects, and peristaltic pumping governs the overall transport dynamics.

Fig. 5e illustrates the influence of the slenderness parameter (β) on the pressure gradient within the tube. Physically, an increase in β signifies longer or more elongated cilia, which enhance resistance to flow in the central region. This leads to a steeper axial pressure gradient along the tube's core. However, near the tube walls, the opposite effect is observed-the pressure gradient decreases. This suggests that beyond a

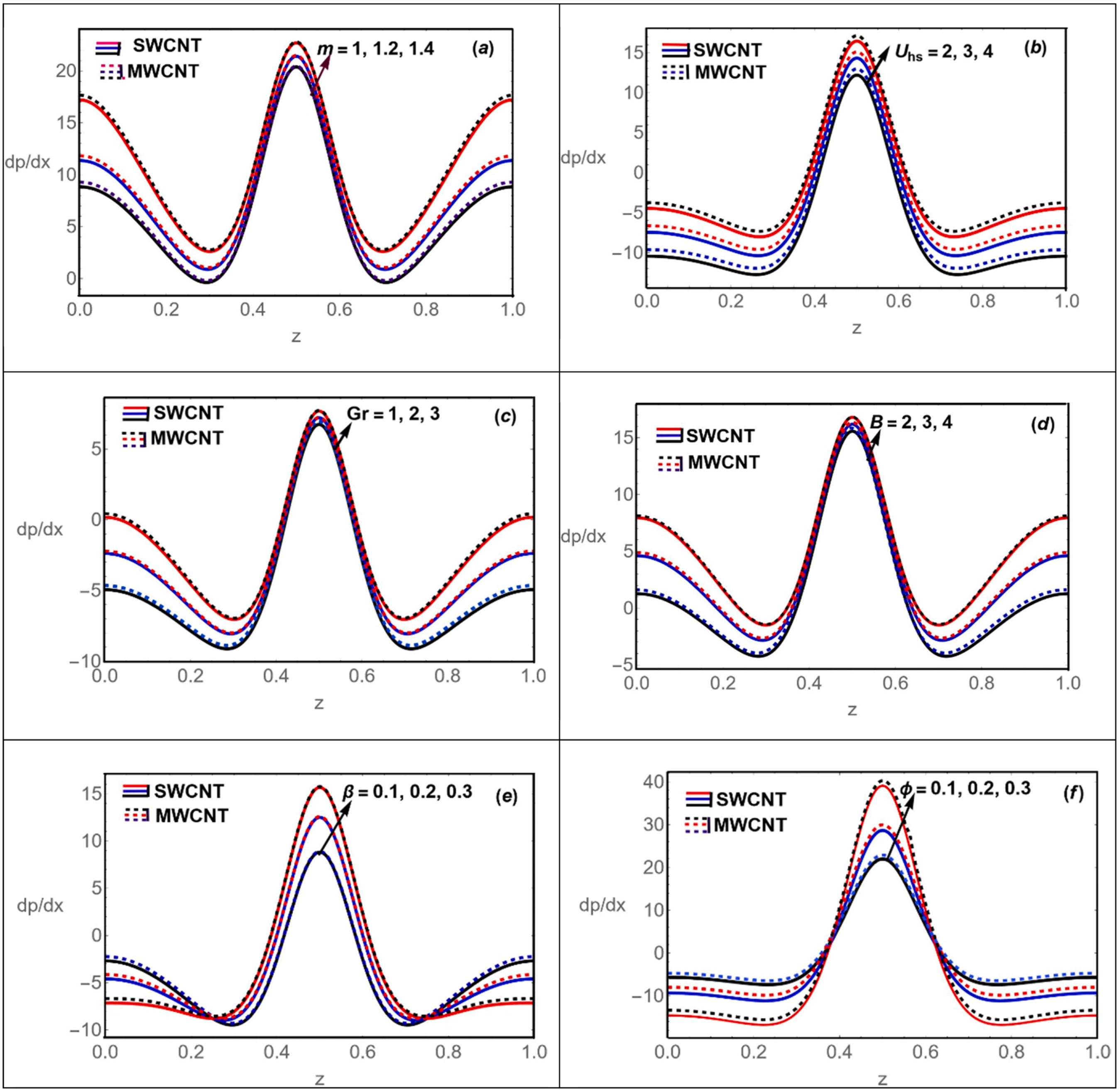

Fig. 5. Axial pressure gradient distributions with variation in (a), electro-osmotic parameter (m), (b) Helmholtz-Smoluchowski parameter U_{hs}, (c) thermal Grashof number Gr, (d) thermal source parameter (B),(e), Slenderness parameter (β), (f), the CNT volume fraction (ϕ), and for fixed values of other parameters $(\widetilde{Q} = 0.1, t = 0.5, \lambda_1 = 2, z = 0.5, L = 1, \alpha = 0.2,\ \alpha_1 = 0.2)$.

certain length, the cilia's ability to influence fluid movement in the peripheral region diminishes, reinforcing the existence of an upper limit to their effective reach into the core flow zone. Larger cilia while inducing flow deceleration in the core zone (as computed earlier) however are beneficial to mobilizing larger axial pressure gradients in the core flow. Fig 5(f) shows that increasing CNT volume fraction(ϕ) increases the pressure gradient. Effects of MWCNT increases the pressure gradient more prominently in comparison with single wall carbon nano tube SWCNT.

4.4. Pumping characteristics

In bio-inspired peristaltic micropumps, and natural mechanisms e.g. human swallowing and digestion, peristaltic flow is very efficient at propelling liquids. The pressure rise ensures efficient transport of nutrients and waste products. The significance of pressure rise in peristaltic flow lies in its ability to facilitate fluid transportation, mixing, metering, dispensing, contamination control, gentle handling of fluids, and its relevance in various biological and industrial processes. In order to properly understand pumping dynamics, the pressure rise per wavelength is crucial, as depicted in Fig. 6(a)–(e). Fig. 6(a) and (b) illustrate the profile for the pressure rise of the ionic nanofluid versus the time-averaged volume flow rate $\widetilde{Q}$ for various values of the Helmholtz-Smoluchowski velocity (U_{hs}) and Debye- Hückel parameter i.e. inverse EDL parameter (m). It becomes evident that the pressure rise follows a linear trend with flow rate and diminishes as the flow rate increases. Fig. 6(a) clearly illustrates that an increase in the Debye–Hückel

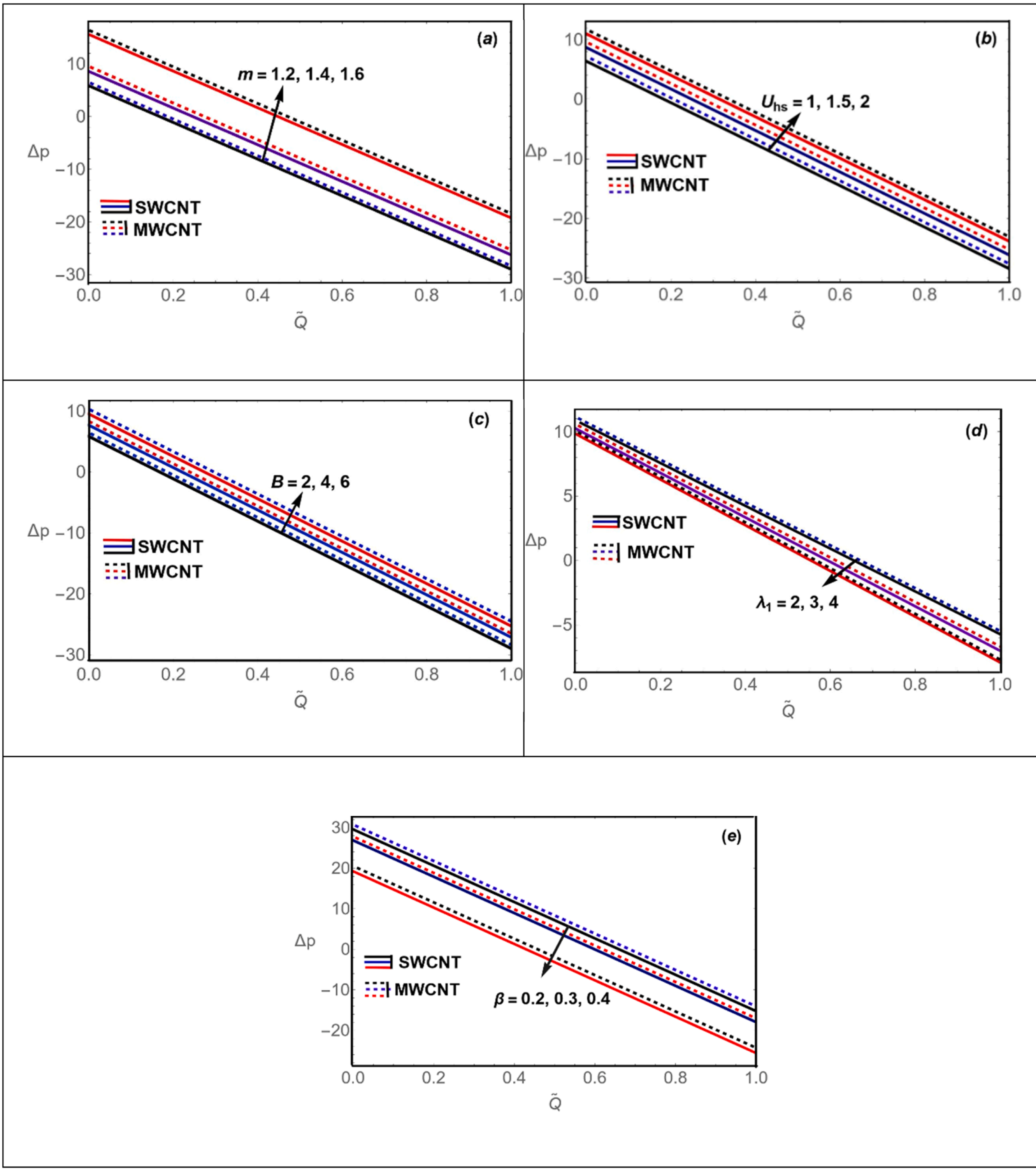

Fig. 6. Pressure rise versus mean flow rate $\widetilde{Q}$ with variation in (a), electro-osmotic parameter(m), (b) Helmholtz-Smoluchowski parameter (U_{hs}) (c) Source sink parameter(B), (d) viscoelastic material parameter(λ_1), (e), and Cilia parameter (β) and for fixed values of other parameters($\phi = 0.2, t = 0.5, Gr = 4,\ z = 0.5, L = 1,$ $\alpha_1 = 0.2$).

parameter leads to a notable rise in pressure. This trend can be attributed to the reduction in the characteristic thickness of the electric double layer (EDL), which enhances the electrostatic interactions within the system. Furthermore, when comparing different nanostructures, multi-walled carbon nanotubes (*MWCNTs*) exhibit significantly higher pressure rise magnitudes than single-walled carbon nanotubes (*SWCNTs*). This difference arises due to the additional concentric graphene layers in *MWCNTs*, which contribute to an increased surface area and a more pronounced influence of electrokinetic effects on fluid flow. The impact of Helmholtz-Smoluchowski velocity is illustrated in Fig. 6(b). The Helmholtz-Smoluchowski velocity influences fluid motion in a manner similar to the Debye–Hückel parameter, affecting all three key pumping regions. In the retrograde pumping zone (where the pressure difference, Δp, is positive and the flow rate, $\widetilde{Q}$, is negative), the electrokinetic effects oppose the natural flow direction, causing fluid to move in reverse. In the peristaltic pumping region (where both Δp and $\widetilde{Q}$ are positive), the electrokinetic influence enhances the forward movement of the fluid, reinforcing the natural pumping action. In the augmented pumping zone (where Δp is negative and $\widetilde{Q}$ is positive), the electrokinetic effects assist fluid motion even against a pressure gradient, effectively increasing the overall flow rate. These interactions illustrate how surface charge and electrokinetic effects modify fluid transport in microfluidic and biological systems. In Fig. 6(c), we can see that the peristaltic pumping rate of the ionic nanofluid increases with the heat source parameter, B. This is because the thermal energy from the heat source boosts the kinetic energy of the fluid particles. As the temperature rises, the viscosity of the ionic nanofluid decreases due to thermal thinning effects, reducing flow resistance. This allows the peristaltic waves to drive the fluid more effectively, resulting in a higher pumping rate. Fig. 6(d) shows that as the second-grade material parameter λ_1 increases, the pressure rise also increases consistently. This parameter, given by $\lambda_1 = \frac{c\widetilde{\lambda_1}}{\lambda}$, represents the ratio of relaxation time to retardation time in the fluid. It appears in the modified fractional viscoelastic shear term of the momentum Eq. (21), influencing how the fluid responds to applied forces. Physically, a higher λ_1 means that the fluid takes longer to return to its original state after being stressed. This delayed relaxation reduces the axial pressure gradient, meaning that less force is required to sustain flow. As a result, the pressure rise becomes more pronounced with increasing λ_1, reflecting the greater resistance of the fluid to deformation and its slower recovery after stress is removed. Fig. 6(e) clearly demonstrates that as the slenderness parameter (β) increases, the magnitude of pressure rise per wavelength decreases. Although longer cilia enhance axial pressure gradients in the central region, they simultaneously reduce the overall pressure rise as the volumetric flow rate increases. This behavior suggests that while extended cilia generate localized resistance, they also facilitate smoother fluid transport, thereby lowering the net pressure rise. Furthermore, multi-walled carbon nanotubes (*MWCNTs*) consistently exhibit higher pressure rise magnitudes (Δp) compared to single-walled carbon nanotubes (*SWCNTs*), indicating their superior ability to influence fluid dynamics within the system.

4.5. *Trapping characteristics (Bolus dynamics)*

The trapping phenomenon can be studied by computing streamline distributions which enable a deeper understanding of how fluid zones (boluses) are formed within the peristaltic regime and how matter is transported, such as cells, waste materials, robotic ionic fluids etc., in micro-peristaltic pump systems. This is relevant in biological and biomedical applications where controlled transport of materials is critical. It is also relevant to cell sorting or tissue engineering. Mixing

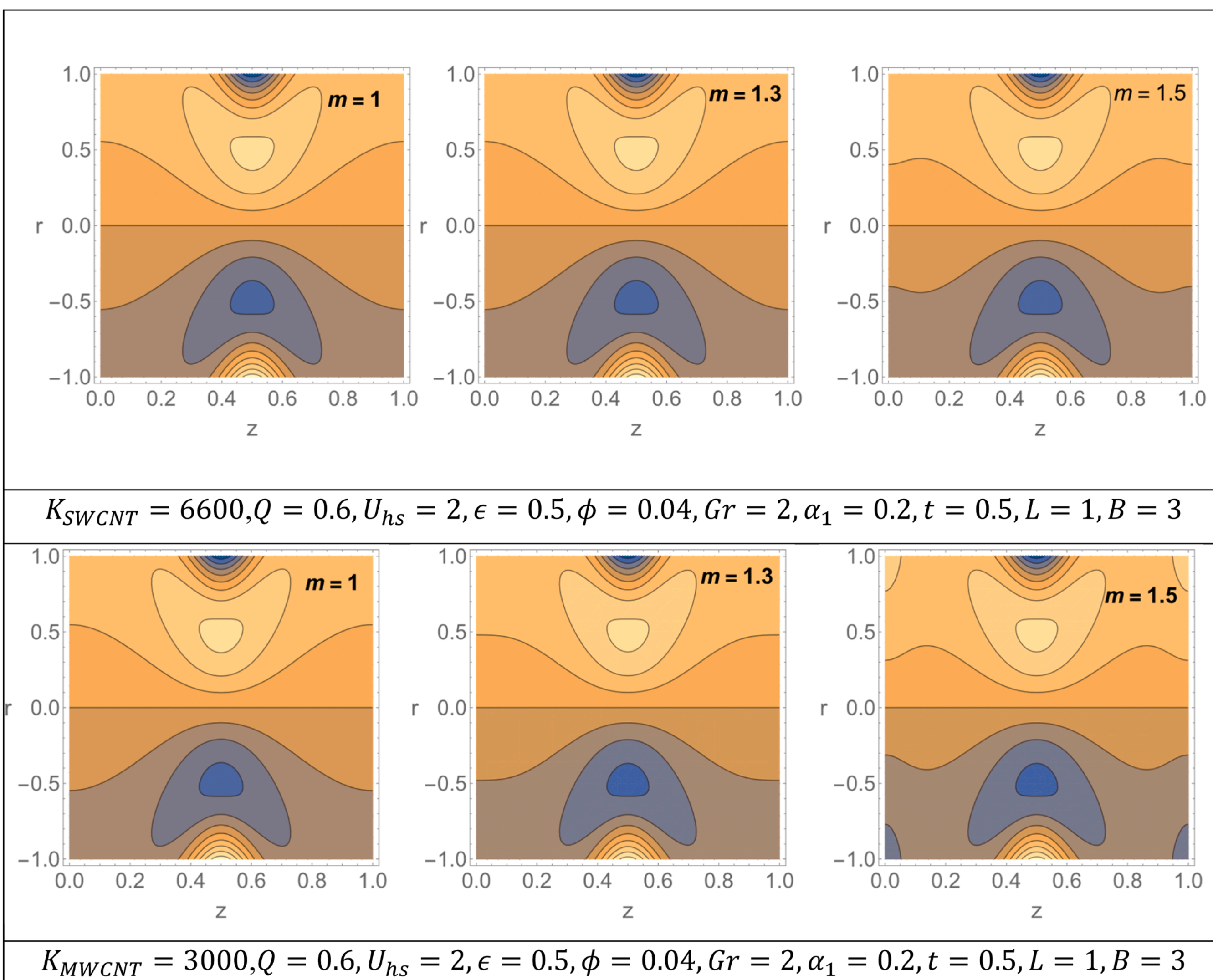

Fig. 7. Streamlines with variation in electro-osmotic parameter (m) and thermal conductivity of MWCNT (K_{MWCNT}) and SWCNT (K_{SWCNT}).

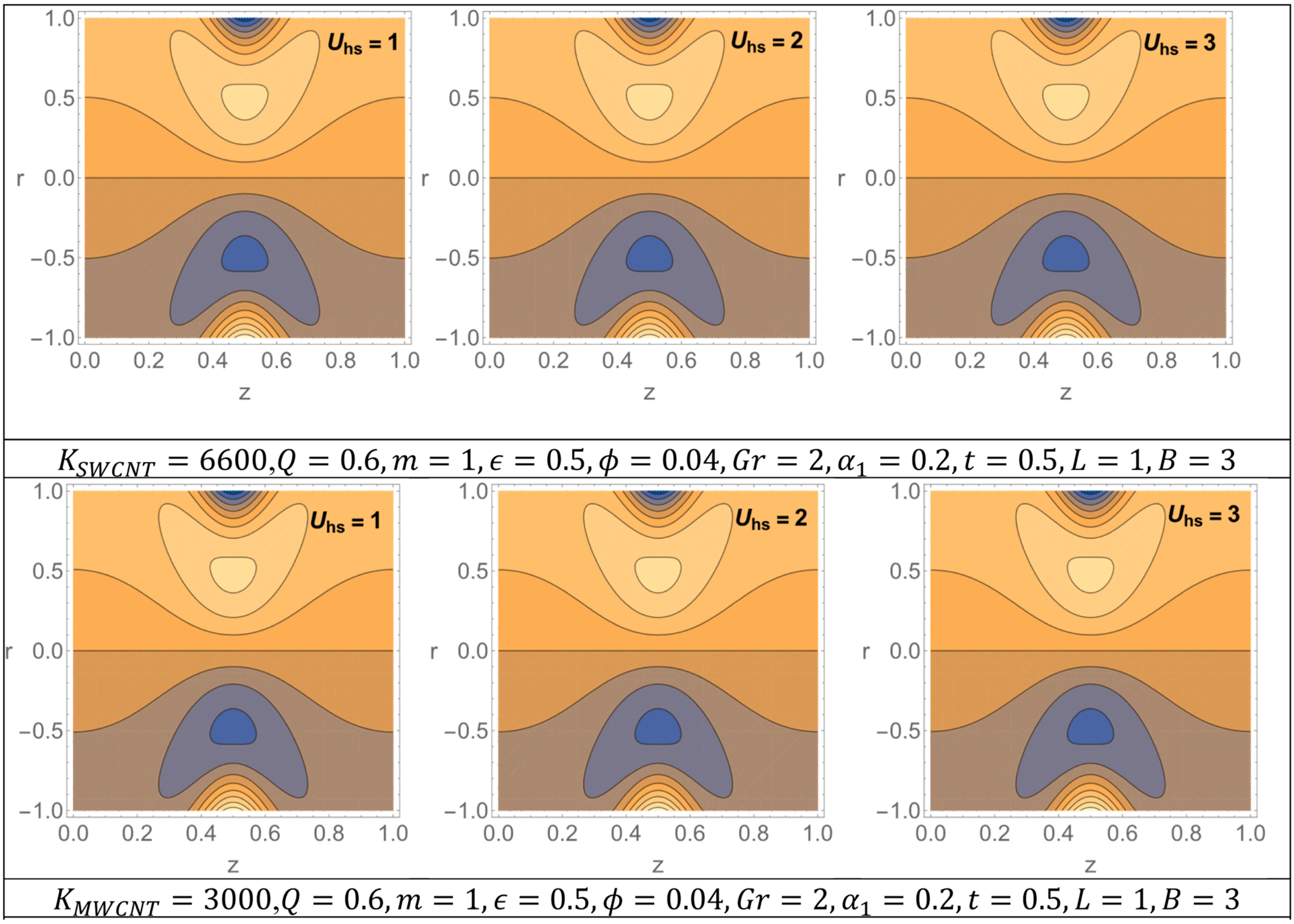

Fig. 8. Streamlines computed with different Hemholtz-Smoluchowski velocity U_{hs} and thermal conductivity of MWCNT (K_{MWCNT}) and SWCNT (K_{SWCNT}).

enhancement and controlled manipulation of substances within microfluidic systems can be optimized with bolus dynamics analysis.

Figs. 7–9 show the streamlines pattern for SWCNT and MWCNT flow against different values of electro-osmotic parameter m, Helmholtz-Smoluchowski velocity parameter U_{hs}. In all three plots we also consider the variation in thermal conductivity of MWCNT (K_{MWCNT}) for the top row of streamlines and SWCNT (K_{SWCNT}) for the base row. Fig. 7 show the streamlines pattern for different values of electro-osmotic parameter m and thermal conductivity of MWCNT (K_{MWCNT}) for the top row of streamlines and SWCNT (K_{SWCNT}) for the base row. The fluid is transported via the peristaltic action with the assistance of the ciliated boundary walls, as seen by the trapped bolus inside the streamlines. A dual bolus structure is computed, and the magnitude of the upper and lower bolus is enhanced with increasing electro-osmotic parameter m. A very slightly larger bolus structure is observed for the SWCNT (K_{SWCNT}) relative to the MWCNT (K_{MWCNT}). In Fig. 8 it is observed that the size of the dual trapped boluses increases with the increase in the Helmholtz-Smoluchowski velocity, U_{hs} from negative (opposing electrical field) to positive values (assisted electrical field), although the number of boluses is not modified. Also, the boluses are not fully formed and morph from the upper and lower walls expanding into the core zone. Greater streamline intensities are computed for the *SWCNT* case (lower row) compared with the *MWCNT* case (upper row). The interplay between electro-osmotic forces (U_{hs}) and *CNT* nanofluid properties determines the efficiency of bolus trapping and drug transport**.** Electro-osmotic effects dominate bolus expansion and movement**,** while *CNT* properties influence viscosity and diffusion control**.** These insights are crucial for designing precise drug delivery mechanisms**,** ensuring efficient, targeted transport in microfluidic and biomedical system**.** Based on these findings, optimal control of bolus formation for drug delivery applications can be achieved by: Tuning the applied electric field (U_{hs}) to control bolus expansion and transport speed. Optimizing *CNT* concentration to balance viscoelastic properties without suppressing electro-osmotic effects. Adjusting peristaltic wave parameters to ensure stable bolus transport in microfluidic or biomedical applications. Fig. 9 also presents streamlines for increasing values of the CNT volume fraction ϕ and again thermal conductivity of MWCNT (K_{MWCNT}) for the top row of streamlines and SWCNT (K_{SWCNT}) for the base row. A decrease in the size of trapped zones (boluses) is noticed at the upper and lower walls of the microtube with greater volume fraction, although again the partially formed dual upper and lower boluses expand considerably in the core zone. There is an expansion in bolus structure with increasing volume fraction from 0.3 through 0.4 to 0.5, although very little difference is computed in trapped zone structures for the (K_{SWCNT}) and SWCNT (K_{SWCNT}) cases. In targeted cancer therapy**,** where nanocarriers deliver chemotherapy drugs, adjusting ϕ could control how long drugs remain in specific regions, optimizing treatment efficacy while minimizing side effects. The dominance of electro kinetic effects (m, U_{hs}) over thermal conductivity (K_{MWCNt}, K_{SWCNT}) indicates that electric field modulation is more effective for controlling particle transport than modifying *CNT* composition. This is critical in electro-osmotic pumps, where fluid flow is driven by an applied electric field.

The validation of the current model is demonstrated in Fig. 10 and Table 2, which depicts the axial velocity distribution. The results in Fig. 10 indicate a close alignment between the present model and the results of Akbar and Butt [40] for different volume flow rates ($\widetilde{Q}$),

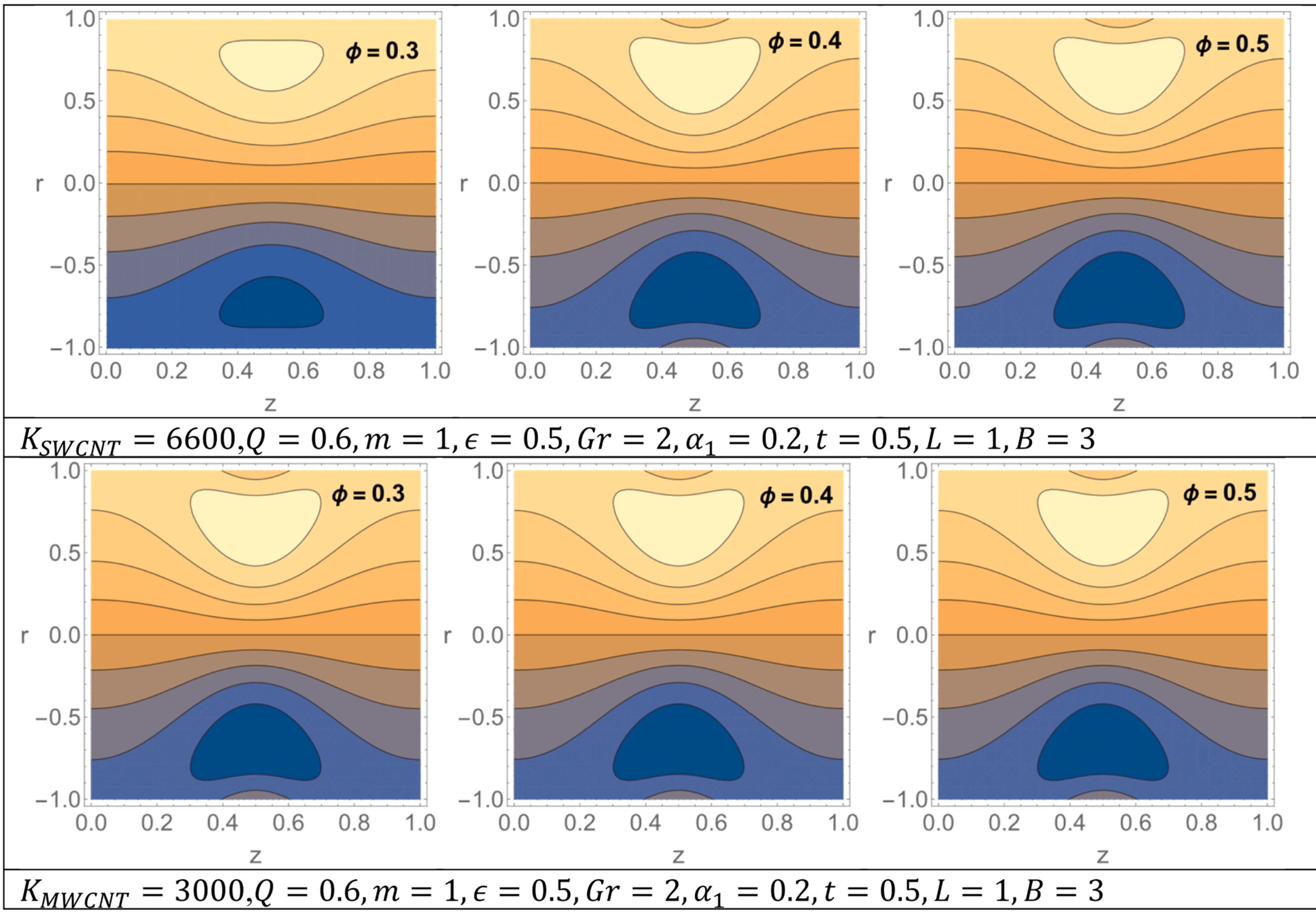

Fig. 9. Streamline for carbon nanotube volume fraction (ϕ) and thermal conductivity of MWCNT (K_{MWCNT}) and SWCNT (K_{SWCNT}).

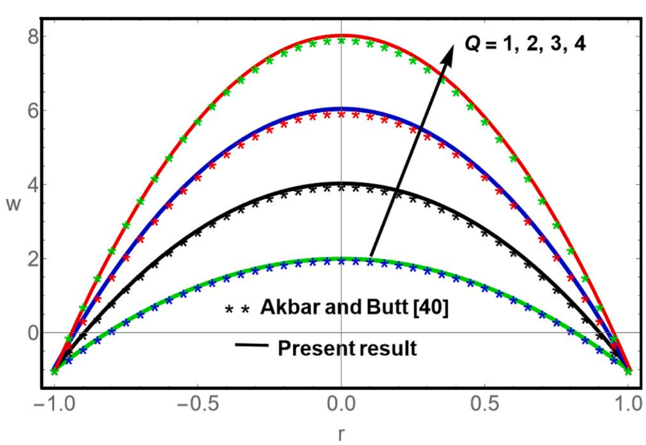

Fig. 10. Comparison of present work when $m = 0,\ U_{Hs} = 0.\phi = 0$.

validating the present model and its results.

5. Conclusions

A mathematical model has been developed to study electro-osmotic peristaltic streaming flow of a fractional second grade ionic nanofluid in a ciliated tube, considering metachronal propulsion with an elliptic cilia model. The model includes analysis of a sinusoidal peristaltic wave form and investigates the effects of single-walled carbon nanotubes (*SWCNTs*) and multi-walled carbon nanotubes (*MWCNTs*). The fractional model uses Caputo's definition, and heat generation and thermal buoyancy are considered. The Debye- Hückel linearization approximation is used for the electro-osmotic model with lubrication theory in the wave reference frame. Analytical solutions are obtained for various parameters such as electrical potential, axial velocity, temperature, volumetric flow rate, axial pressure gradient, pressure rise, and friction force. Numerical evaluations in **Mathematica** software show the combined effects of peristalsis, *CNT* type and volume fraction, and electro-osmosis on hydrodynamic and thermal characteristics. The study provides insights

Table 2
Comparison of velocity profiles with Akbar and Butt [40] for various values of $\tilde{Q}$.

Akbar and Butt [40]				Present work $m = 0, U_{hs} = 0$			
$Q = 1$	$Q = 2$	$Q = 3$	$Q = 4$	$\tilde{Q} = 1$	$\tilde{Q} = 2$	$\tilde{Q} = 3$	$\tilde{Q} = 4$
−1	−1	−1	−1	−1	−1	−1	−1
1.24702	2.74503	4.24304	5.74105	1.250	2.750	4.250	5.75
1.98417	3.97361	5.96306	7.95251	2	4	6	8
1.24702	2.74503	4.24304	5.74105	1.250	2.750	2.750	2.750
−1	−1	−1	−1	−1	−1	−1	−1

into the behavior of nanofluid transport in ciliated tubes under electrokinetic effects.

i] The axial velocity decreases in the core region of the duct when the Helmholtz-Smoluchowski parameter (U_{hs}) is negative and there is a reverse axial electrical field. Conversely, the velocity increases when the parameter is positive and the electrical field is aligned axially. The opposite effect is observed in the peripheral zones.
ii] With elevation in cilia length (β) parameter and electro-osmotic parameter (m) the core axial flow is consistently suppressed whereas the peripheral flow is accelerated.
iii] Increasing thermal source parameter (B), thermal Grashof number (Gr) and nanotube volume fraction (ϕ) significantly elevate the axial velocity magnitudes in the central (core) region.
iv] Invariably, slightly greater axial velocities are computed for *MWCNTs* relative to *SWCNTs*.
v] The magnitude of dual trapped boluses increases with the increase in the Helmholtz-Smoluchowski velocity, U_{hs} from negative (opposing electrical field) to positive values (assisted electrical field), although the number of boluses is not modified.
vi] A marginally larger bolus structure is observed for the SWCNT (K_{SWCNT}) case relative to the MWCNT (K_{MWCNT}) case.
vii] The primary alteration in bolus structures is attributed to the effects of electrical potential and the electric field (m, U_{hs}), rather than the thermal conductivity of carbon nanotubes (CNTs) or their volumetric proportion (percentage doping, ϕ).
viii] Temperature is strongly boosted across the duct with increasing thermal source/sink parameter (B), whereas it is significantly depleted with carbon nanotube (*CNT*) volume fraction (ϕ) and *MWCNTs* generally achieve higher temperatures than *SWCNTs*.
ix] Axial pressure gradient is consistently elevated with electro-osmotic parameter i.e. inverse Debye length (m), positive Helmholtz-Smoluchowski parameter (U_{hs}), Grashof number (Gr), thermal source parameter and cilia length (β) whereas it is suppressed with higher carbon nanotube (CNT) volume fraction (ϕ).
x] Pressure rise exhibits an inverse linear relationship with mean flow rate $\widetilde{Q}$ and the former is strongly boosted with electro-osmotic parameter (m), positive Helmholtz-Smoluchowski parameter U_{hs} and thermal source (B) whereas pressure rise is strongly suppressed with increasing viscoelastic material parameter (λ_1) and cilia length (β).

The study reveals fascinating aspects of cilia-peristaltic electro-osmotic thermal pumping in micro-tube systems, relevant to bio-microfluidics and hazardous waste transport. Future research should incorporate Brownian motion and thermophoresis effects to better simulate nanoparticle transport in bio-fluids. Alternative non-Newtonian models like Pan-Thien-Tanner viscoelastic, Eringen micropolar, and couple stress theories could be explored. This study serves as a foundation for investigating bioheat transfer in electro-osmotic nanofluid pumping. Further studies should integrate nonlinear electro-osmotic forces and fluid dynamics for a more realistic depiction of biological interactions. Expanding to multiphase fluid models could enhance understanding of blood cell-plasma interactions.

Funding

No funding.

Ethics approval

Not applicable

CRediT authorship contribution statement

Mahadev M Channakote: Writing – original draft, Methodology, Investigation. **Shekar Marudappa:** Visualization, Validation, Software. **O. Anwar Bég:** Writing – review & editing. **Mahesha Narayana:** Writing – review & editing, Visualization. **C. Siddabasappa:** Writing – review & editing, Software, Conceptualization.

Declaration of competing interest

The authors declare that the research was conducted in the absence of any commercial or financial relationships that could be conducted as a potential conflict of interest.

Data availability

The authors do not have permission to share data.

References

[1] F. Yin, Y. Fung, Comparison of theory and experiment in peristaltic transport, J. Fluid Mech. 47 (1971) 93–112.
[2] A.H. Shapiro, M.Y. Jaffrin, S.L. Weinberg, Peristaltic pumping with long wavelengths at low reynolds number, J. Fluid Mech. 37 (1969) 799–825.
[3] V.P. Rathod, M.M. Channakote, A study of ureteral peristalsis in cylindrical tube through porous medium, Adv. Appl. Sci. Res. 2 (3) (2011) 134–140.
[4] V.K. Narla, D. Tripathi, O. Anwar Bég, A. Kadir, Modelling transient magnetohydrodynamic peristaltic pumping of electroconductive viscoelastic fluids through a deformable curved channel, J. Eng. Math. 111 (2018) 127–143.
[5] M. Ajithkumar, P. Lakshminarayana, D. Tripathi, S. Kuharat, O. Anwar Bég, Catalytic effects on radiative peristaltic flow of Jeffrey fluid through a flexible divergent duct with an aligned magnetic field: *application in biomimetic pumps for hazardous materials*, Ther. Sci. Eng. Prog. (17) (2024), https://doi.org/10.1016/j.tsep.2024.102476.
[6] V.P. Rathod, M. Mahadev, Effect of magnetic field on ureteral peristalsis in cylindrical tube, J. Ultra Sci. Phy. Sci. 23 (1) (2016) 135–142.
[7] T. Hayat, M. Ibtesam, S.A. Khan, B. Ahmed, Role of silver nanoparticle in thermal energy process regulated by peristalsis, Result. Eng. 24 (2024) 103062.
[8] R. Choudhari, H. Vaidya, K.V. Prasad, M. Gudekote, M. Ijaz Khan, M. Akermi, R. Hassani, H.A. Hejazi, S. Ali, Analysis of peristalsis blood flow mechanism using non-Newtonian fluid and variable liquid characteristics, Result. Eng. 21 (2024) 101842.
[9] D. Tripathi, O. Anwar Bég, P.K. Gupta, G. Radhakrishnamacharya, J. Mazumdar, DTM simulation of peristaltic viscoelastic biofluid flow in asymmetric porous media: a digestive transport model, J. Bion. Eng. 12 (4) (2015) 1–13.
[10] N. Ali, K. Javid, M. Sajid, O. Anwar Bég, Numerical simulation of peristaltic flow of a biorheological fluid with shear-dependent viscosity in a curved channel, Compt. Meth. Biomech. and Biomed. Eng. 19 (6) (2016) 614–627.
[11] D. Khan, K. Kenneth Asogwa, T. Alqahtani, S. Algarni, S. Alqahtani, M.A. Akbar, A generalized two-phase free convection flow of dusty Jeffrey fluid between infinite vertical parallel plates with heat transfer, J. Math. 2022 (2022) 8470139, https://doi.org/10.1155/2022/8470139.
[12] D. Khan, P. Kumam, W. Watthayu, F. Jarad, Exploring the potential of heat transfer and entropy generation of generalized dusty tetra hybrid nanofluid in a microchannel, Chin. J. Phys. 89 (2024) 1009–1023.
[13] S.K. Asha, C.K. Deepa, Entropy generation for peristaltic blood flow of a magneto-micropolar fluid with thermal radiation in a tapered asymmetric channel, Result. Eng. 3 (2019) 100024.
[14] M.M. Channakote, D.V. Kalse, Combined convective and viscous dissipation effects on peristaltic flow of Ellis fluid in a non-uniform tube, J. Naval Arch. Mar. Eng. 19 (2022) 1–12, https://doi.org/10.3329/jname.v.19.55052.
[15] A. Imran, M.A.Z. Raja, S.E. Awan, M. Shoaib, Analysis of radiative heat transfer on electro-osmotic magneto nanofluid flow through ciliary propulsion, Z. Angew. Math. Mech. (2024) e202300689.
[16] A. Imran, M.A.Z. Raja, M. Shoaib, M. Zeb, Kottak karan Sooppy Nisar, electro-osmotic transport of a Williamson fluid within a ciliated microchannel with heat transfer analysis, Case Stud. Therm. Eng. 45 (2023) 102904.
[17] M.M. Channakote, D.V. Kalse, Heat transfer in peristaltic motion of Rabinowitsch fluid in a channel with permeable wall, Appl. Appl. Math: An Int. J. 16 (2) (2021) 1–20.
[18] M.M. Channakote, C. Siddabasappa, Heat and mass transfer analysis on peristaltic transport of PTT fluid with wall properties, Latin Amer. Appl. Res 54 (4) (2024) 545–553.
[19] M.A. Elogail, Peristaltic flow of a hyperbolic tangent fluid with variable parameters, Result. Eng. 17 (2023) 100955.
[20] A.M. Abd-All, E.N. Thabet, F.S. Bayones, A.M. Alsharif, Heat transfer in a non-uniform channel on MHD peristaltic flow of a fractional Jeffrey model via porous medium, Ind. J. Phys. 97 (6) (2022) 1799–1809.

[21] D. Khan, A.u. Rahman, P. Kumam, W. Watthayu, A fractional analysis of hyperthermia therapy on breast cancer in a porous medium along with radiative microwave heating, Fract. Fract. 6 (2022) 82.
[22] O. Anwar Bég, D.E. Sanchez Espinoza, A. Sohail, T.A. Bég, A. Kadir, Experimental study of improved rheology and lubricity of drilling fluids enhanced with nanoparticles, Appl. Nanosci. 8 (2018) 1069–1090.
[23] W.F. Alfwzan, A. Imran, F.M. Allehiany, M.S. Aldhabani, A mathematical model for cilia actuated transport of gold–Silver hybrid nanofluid EMHD flow with activation energy phenomena, Case Stud. Therm. Eng. 49 (2023) 103252.
[24] A. Rehman, D. Khan, R. Jan, A. Aloqaily, N. Mlaiki, Scientific exploring of Marangoni convection in stagnation point flow of blood-based carbon nanotubes nanofluid over an unsteady stretching surface, Int. J. Thermofluid. 20 (2023) 100470.
[25] Z.R. Cui, R.J. Mumper, Microparticles and nanoparticles as delivery systems for DNA vaccines, Crit. Rev. Ther. Drug. Carr. Syst. 20 (2003) 103–137.
[26] S.U.S. Choi, Enhancing thermal conductivity of fluids with nanoparticles. ASME FED, in: Proceedings of the ASME Int. Mech. Eng. Cong. Expos, San Francisco, USA 66, 1995.
[27] J. Buongiorno, Convective transport in nanofluids, ASME J. Heat Transf. 128 (2005) 240–250.
[28] D. Tripathi, Bég, O. Anwar, A study on peristaltic flow of nano fluids: application in drug delivery systems, Int. J. Heat Mass Transf. 70 (2014) 61–70.
[29] S. Nadeem, A. Riaz, R. Ellahi, N.S. Akbar, Mathematical model for the peristaltic flow of nano fluid through eccentric tubes comprising porous medium, Appl. Nanosci. 4 (2014) 733–743, https://doi.org/10.1007/s13204-013-0249-2.
[30] D. Tripathi, S. Bhushan, O.A. Bég, et al., Transient peristaltic diffusion of Nano fluids: a model of micropumps in medical engineering, J. Hydrodyn. 30 (2018) 1001–1011, https://doi.org/10.1007/s42241-018-0140-4.
[31] J. Prakash, E.P. Siva, D. Tripathi, S. Kuharat, O. Anwar Bég, Peristaltic pumping of magnetic nanofluids with thermal radiation and temperature-dependent viscosity effects: modelling a solar magneto-biomimetic nano pump, Renew. Energy 133 (2019) 1308–1326.
[32] A. Rehman, D. Khan, R. Jan, A. Aloqaily, N. Mlaiki, Scientific exploring of Marangoni convection in stagnation point flow of blood-based carbon nanotubes nanofluid over an unsteady stretching surface, Int. J. Thermofield. 20 (2023) 100470.
[33] I. Mahariq, H. Dolat khan, M. Ali Ghazwani, A. Shah, Enhancing heat and mass transfer in MHD tetra hybrid nanofluid on solar collector plate through fractal operator analysis, Result. Eng. 24 (2024) 103163.
[34] M. Waqas, O. Anwar Bég, S. Kuharat, et al., Numerical study of dissipative SW/MWCNT-nanofluid coating flow from a stretching wall to a porous medium with shape factor effects, Int. J. Hydrog. Energy 48 (2023) 34536–34550.
[35] S. Nadeem, S.. Hina, Exploration of single wall carbon nanotubes for the peristaltic motion in a curved channel with variable viscosity, J Braz. Soc. Mech. Sci. Eng. 39 (2017) 117–125.
[36] S. Iqra Shahzadi, F.R. Nadeem, Simultaneous effects of single wall carbon nanotube and effective variable viscosity for peristaltic flow through annulus having permeable walls, Result. Phys. 7 (2017) 667–676.
[37] M.A. Sleigh, The Biology of Cilia and Flagella, MacMillan, New York, USA, 1962.
[38] J. Blake, A spherical envelope approach to ciliary propulsion, J. Fluid Mech. 46 (1971) 199–208.
[39] M. Almheidat, M. Alqudah, A. Imran, F.M. Allehiany, M.M. Alqarni, M. S. Alqurashi, E.E. Mahmoud, Thermal analysis using Prandtl nanofluid in a non-uniform channel: computational paradigm focusing on complex cilia waves, Case Stud. Therm. Eng. 68 (2025) 105872.
[40] K. Ramesh, D. Tripathi, O. Anwar Bég, Cilia-assisted hydromagnetic pumping of bio rheological couple stress fluids, Propuls. Power Res. 8 (3) (2019) 221–233.
[41] A.W. Butt, N.S. Akbar, N. Ahmad Mir, Heat transfer analysis of the peristaltic flow of a Phan-Thien–Tanner fluid model due to metachronal wave of cilia, Biomech. Model. Mechanobiol. 19 (2020) 925–1933.
[42] A.W. Butt, N.S. Akbar, Heat transfer analysis of viscoelastic fluid due to metachronal wave of cilia, Int. J. Biomath 7 (6) (2014) 1450066.
[43] S. Hanasoge, M.R. Ballard, P.J. Hesketh, A. Alexeev, Asymmetric motion of magnetically actuated artificial cilia, Lab. Chip. 17 (2017) 3138–3145.
[44] N.S. Akbar, D. Tripathi, O. Anwar Bég, Z.H. Khan, MHD dissipative flow and heat transfer of Casson fluids due to metachronal wave propulsion of beating cilia with thermal and velocity slip effects under an oblique magnetic field, Acta Astronaut. 128 (2016) 1–12.
[45] S.I. Abdelsalam, M.M. Bhatti, A. Zeeshan, A. Riaz, O. Anwar Bég, Metachronal propulsion of magnetized particle-fluid suspension in a ciliated channel with heat and mass transfer, Physi. Scripta 94 (13pp) (2019) 115301.
[46] N. Manzoor, O. Anwar Bég, K. Maqbool, S. Shaheen, Mathematical modelling of ciliary propulsion of an electrically conducting Johnson-Segalman physiological fluid in a channel with slip, Comp. Meth. Biomech. Biomed. Eng. 22 (2019) 685–695.
[47] N.S. Akbar, D. Tripathi, Z.H. Khan, O. Anwar Bég, Mathematical modelling of pressure-driven micropolar biological flow due to metachronal wave propulsion of beating cilia, Math. Biosc. 301 (2018) 121–128.
[48] N.S. Akbar, M. Shoaib, D. Tripathi, S. Bhushan, O. Anwar Bég, Analytical approach for entropy generation and heat transfer analysis of CNT-nanofluids through ciliated porous medium, J. Hydrodynamics B 30 (2) (2018) 1–11.
[49] A.W. Butt, N.S. Akbar, R. Mehmood, S. Farooq, Thermally conductive electro-osmotic propulsive pressure driven peristaltic streaming flow study with a suspended nanomaterial in a micro-ciliated tube, Front. Mater. 9 (2022) 1059816.
[50] S.I. Abdelsalam, M.M. Bhatti, A. Zeeshan, A. Riaz, O. Anwar Bég, Metachronal propulsion of magnetized particle-fluid suspension in a ciliated channel with heat and mass transfer, Phys. Scripta 94 (13pp) (2019) 115301.
[51] S. Chakraborty, Augmentation of peristaltic micro flows through electro-osmotic mechanisms, J. Phy.D Appl. Phy. 39 (2006) 5356.
[52] D. Tripathi, A. Yadav, O. Anwar Bég, Electro-osmotic flow of couple stress fluids in a micro-channel propagated by peristalsis, Europ. Phys. J. Plus *(Italy)* (2017) 132173–132185.
[53] M.M. Channakote, M. Shekar, Peristalsis of electro-osmotic jeffery fluid in the presence of thermal radiation and heat transfer with the permeable wall, Jord. J. Math. Stat. 17 (2024) 1–12.
[54] N. Ali, S. Hussain, K. Ullah, O. Anwar Bég, Mathematical modelling of Ellis/newtonian two-fluid electro-osmotic peristaltic pumping in an axisymmetric tube, Eur. Phys. J. Plus 134 (2019) 1–18.
[55] D. Tripathi, A. Sharma, O. Anwar Bég, Electro-thermal transport of nano-fluids via peristaltic pumping in a finite micro-channel: *effects of joule heating and Helmholtz-Smoluchowski velocity*, Int. J. Heat Mass Transf. 111 (2017) 138–149.
[56] J. Prakash, E.P. Siva, D. Tripathi, O. Anwar Bég, Thermal slip and radiative heat transfer effects on electro-osmotic magneto nano liquid peristaltic propulsion through a microchannel, Heat Transf. 48 (12) (2019) 1–27.
[57] D. Tripathi, A. Sharma, O. Anwar Bég, Joule heating and buoyancy effects in electro-osmotic peristaltic transport of nanofluids through a microchannel with complex wave propagation, Adv. Powder Technol. 29 (2018) 639–653.
[58] A. Imran, M. Abbas, S.E. Awan, M. Shoaib, M.A. Raja, Electro osmotic flow of nanofluids within a porous symmetric tapered ciliated channel, ZAMM - J. Appl. Math. Mech./Zeitschrift für Angewandte Mathematik und Mechanik 104 (9) (2024) e202300838.
[59] M.M. Channakote, V.K Dilipkumar, S.K Asha, M. Shekar, Peristalsis of fractional second grade fluid in the presence of electro-osmotic phenomenon with heat and mass transfer, J. Adv. Res. Fluid Mech. Ther. Sci. 114 (2) (2024) 50–65.
[60] A.M. Abd Alla, S.M. Abo Dahab, T. Esraa, M.A. Abdelhafez, Peristaltic pump withheat and mass transfer of a fractional second grade fluid through porou medium inside a tube, Sci. Rep. 12 (2022) 10608.
[61] M.M. Channakote, S.K. Asha, Heat transfer and electro-osmotic analysis on peristaltic pumping of a fractional second-grade fluid through a cylindrical tube, Int. J. Comp. Mat. Sci. Eng. 12 (2023) 2350007.
[62] D. Tripathi, Peristaltic flow of a fractional second grade fluid through a cylindrical tube, Therm. Sci. 15 (2011) S167–S173.
[63] M. Hameed, A. Khan, R. Ellahi, M. Raza, Study of magnetic and heat transfer on the peristaltic transport of a fractional second-grade fluid in a vertical tube, Eng. Sci. Tech. Int. J. 18 (2015) 496–502.
[64] V.P. Rathod, M. Mahadev, Interaction of heat transfer and peristaltic pumping of frictional second-grade fluid through a vertical cylindrical tube, Therm. Sci. 18 (2014) 1109–1118.
[65] X. Guo, H. Qi, Analytical solution of electro-osmotic peristalsis of fractional Jeffrey fluid in a micro-channel, Micromach. (Basel) 8 (12) (2017) 341.
[66] D. Tripathi, O. Anwar Bég, Mathematica numerical simulation of peristaltic biophysical transport of a fractional viscoelastic fluid through an inclined cylindrical tube, Comp. Meth. Biomec. Biomed. Eng. 18 (2014) 1–10.
[67] D. Khan, R. Au, P. Kumam, W. Watthayu, A fractional analysis of hyperthermia therapy on breast cancer in a porous medium along with radiative microwave heating, Fract. Fraction. 6 (2) (2022) 82.
[68] D. Kim, W.S. Lee, S. Shin, H.S. Rho, J. Dai, J.Y. Yun, J.W. Hong, Quantitative analysis of pneumatically driven biomimetic micro peristalsis, Sci. Adv. Mater. 6 (11) (2014) 2428–2434.